OAK RIDGE NATIONAL LABORATORY LIBRARIES
3 4456 0549202 6

CENTRAL RESEARCH LIBRARY
DOCUMENT COLLECTION

OAK RIDGE NATIONAL LABORATORY

operated by

UNION CARBIDE CORPORATION

for the

U. S. ATOMIC ENERGY COMMISSION

ORNL-TM-1100

DECLASSIFIED

CLASSIFICATION CHANGED TO:

BY AUTHORITY OF: AECM-2104 a2 BL 8/21/74

BY: BL Rudd

FUELS AND MATERIALS DEVELOPMENT PROGRAM QUARTERLY PROGRESS REPORT FOR PERIOD ENDING MARCH 31, 1965

CENTRAL RESEARCH LIBRARY
DOCUMENT COLLECTION
LIBRARY LOAN COPY
DO NOT TRANSFER TO ANOTHER PERSON
If you wish someone else to see this document, send in name with document and the library will arrange a loan.

NOTICE This document contains information of a preliminary nature and was prepared primarily for internal use at the Oak Ridge National Laboratory. It is subject to revision or correction and therefore does not represent a final report.

[redacted]

LEGAL NOTICE

This report was prepared as an account of Government sponsored work. Neither the United States, nor the Commission, nor any person acting on behalf of the Commission:

A. Makes any warranty or representation, expressed or implied, with respect to the accuracy, completeness, or usefulness of the information contained in this report, or that the use of any information, apparatus, method, or process disclosed in this report may not infringe privately owned rights; or

B. Assumes any liabilities with respect to the use of, or for damages resulting from the use of any information, apparatus, method, or process disclosed in this report.

As used in the above, "person acting on behalf of the Commission" includes any employee or contractor of the Commission, or employee of such contractor, to the extent that such employee or contractor of the Commission, or employee of such contractor prepares, disseminates, or provides access to, any information pursuant to his employment or contract with the Commission, or his employment with such contractor.

[redacted]

ORNL-TM-1100

Contract No. W-7405-eng-26

FUELS AND MATERIALS DEVELOPMENT PROGRAM QUARTERLY PROGRESS REPORT FOR PERIOD ENDING MARCH 31, 1965

Compiled by

P. Patriarca

JUNE 1965

OAK RIDGE NATIONAL LABORATORY
Oak Ridge, Tennessee
operated by
UNION CARBIDE CORPORATION
for the
U. S. ATOMIC ENERGY COMMISSION

OAK RIDGE NATIONAL LABORATORY LIBRARIES

3 4456 0549202 6

[redacted]

[redacted]

FOREWORD

This is the fourth quarterly progress report describing work performed at the Oak Ridge National Laboratory for the Fuels and Materials Development Branch, Division of Reactor Development, U. S. Atomic Energy Commission. The specific programs covered are as follows:

Part I. Metals and Ceramics Division

Program Title	Person in Charge	Principal Investigator(s)
Fuel Element Development	G. M. Adamson, Jr.	C. F. Leitten, Jr. J. P. Hammond
Nondestructive Test Development	D. A. Douglas, Jr.	R. W. McClung
Solid Reaction Studies	C. J. McHargue	T. S. Lundy
Zirconium Metallurgy	C. J. McHargue	M. L. Picklesimer

Part II. Solid State Division

Irradiation Effects on Alloys and Structural Materials	D. S. Billington	M. S. Wechsler

[redacted]

[redacted]

TABLE OF CONTENTS

Page

Summary v

Part I. Metals and Ceramics Division

1. Fuel Element Development 3
   - Direct Thermochemical Conversion of UCl_4 to UO_2 . . 3
   - Deposition of Uranium Compounds by Lithium Reduction of UF_6 4
   - Deposition of Refractory Metals 5
   - Deposition of Refractory Uranium Compounds 6
   - Deposition of Tungsten Alloys 7
   - Deposition of Fine-Grained Tungsten 9
   - Characterization of Al-U_3O_8 Dispersions 11

2. Nondestructive Test Development 18
   - Electromagnetic Test Methods 18
   - Ultrasonic Test Methods 20
     - Nonbond Studies 20
     - Tubing Inspection 20
   - Penetrating Radiation 23
     - Gamma Scintillation Gaging 23
     - X-Ray Microscope 24
   - Inspection Development of Problem Materials 24
   - Remote Inspection Development 24

3. Solid Reaction Studies 26
   - Diffusion of ^{44}Ti in V–20% Ti 26

4. Zirconium Metallurgy 29
   - Anisotropy in Zircaloy-2 29
   - Oxide Film Studies 36
   - Preparation of Single Crystals of Zirconium and Zirconium Alloys 37
   - Zone Refining of Zirconium 37
   - Properties of High-Purity Zirconium 38

[redacted]

[redacted]

Part II. Solid State Division

5. Irradiation Effects on Alloys and Structural Materials . . 43

Low-Temperature Electron Irradiation of a Copper-Nickel Alloy 45

Resistivity Measurements in Fe—3.7 wt % Si 49

Precipitation of Nitrides in Electron Irradiated Iron . 51

Modification of Torsion Pendulum for Strain Relaxation Measurements 54

Dislocation Dynamics in Iron 57

Tensile Tests on Irradiated Iron and Iron Alloys . . . 65

Hydrogen in Steels 74

Rate of Hydrogen Production by Transmutation in Pressure-Vessel Steel 75

The Minimum Neutron Flux Necessary to Produce Hydrogen Attack 76

Hydrogen Permeability of Steel in a Radiation Environment 79

SM-1 Pressure Vessel Surveillance Program 84

Impact Tests on Irradiated Pressure Vessel Steels . . . 85

Hot-Cell Equipment 86

A Converter Facility for Providing Fission-Spectrum Neutrons in the Bulk Shielding Reactor 87

BSR Liquid-Nitrogen-Cooled Cryostat 94

[redacted]

[redacted]

SUMMARY

1. Fuel Element Development

Work on the thermochemical deposition of fuel materials has been expanded. Calculations have been made and likely reactions selected and equipment is being installed for the direct conversion of UCl_4 with oxygen and hydrogen mixtures and also for the reduction of UF_6 with lithium vapor. In the direct conversion of UF_6 to UO_2, it was shown that the stoichiometry of the oxide deposit is a function of the gas-feed rate as well as the oxygen concentration.

We have now developed thermochemical deposition techniques by which tungsten-rhenium alloys may be deposited directly. The use of a small moving hot zone resulted in high metal recoveries and high rhenium deposits; however, homogeneous deposits have not been achieved. A uniform deposit of pure rhenium has been made with lengths up to 12 in.; however, the metal recovery rate is low. When small quantities of vanadium were deposited with tungsten, a marked drop in tungsten recovery was noted and only traces of vanadium remained in the deposit. Whether grain refinement was obtained is not yet known.

Various commercial U_3O_8 powders were characterized for propensity to fragment when fabricated into aluminum-base dispersion fuel plates. Bulk density, surface area, and particle shape were shown to be important considerations, and large differences were found between the various oxides.

2. Nondestructive Test Development

We are developing new techniques and equipment for the nondestructive evaluation of materials and components. The major emphasis has been on eddy-current, ultrasonic, and penetrating-radiation methods.

The mathematical approach using a computer to analyze variations in electromagnetic field parameters has been applied to the problem of shaping the electromagnetic field and eddy-current flow using ferrite around the coil. Continued developments to the phase-sensitive eddy-current instrument has been directed toward improvements to the circuitry to obtain higher frequency, lower distortion operation.

[redacted]

[redacted]

The ultrasonic test developments have included nonbond evaluation using inner diameter probes in tubular fuel elements with dispersion cores. We are continuing to develop calibration curves and techniques for electro-discharge-machining of reference notches in tubing.

Our newly assembled photomultiplier calibration system was checked out successfully and has already shown its value in optimizing scintillation detector performance. We have begun first stages of work toward the use of light pipes for translating scintillations produced in x-ray attenuation gaging. This would have application in fuel homogeneity determinations in hollow fuel tubes. Using available electron optical components, we have begun the assembly of a projection x-ray microscope.

Our work on problem materials has included tantalum-, tungsten-, molybdenum-, nickel-, and niobium-base alloys.

We are in the final stages of mechanical modification of a remote scanning facility designed for the performance of nondestructive testing in a hot cell.

3. Solid Reaction Studies

In the use of high-temperature materials, one problem of concern is the rate of atomic migration in the material. One method of studying this rate of migration involves the use of radioactive tracers of the species of concern. We are reporting work on the vanadium-titanium alloy system, which is part of a continuing effort to understand diffusion behavior in the body-centered cubic systems.

4. Zirconium Metallurgy

Studies have been made of the effect of width-to-thickness ratios on the anisotropy of mechanical properties and strain in sheet-type tensile specimens of highly textured Zircaloy-2. Yield strength was found to increase slightly with decreased cross-sectional area, independent of the width-to-thickness ratio. Ultimate strengths, elongations at maximum load, and reductions of area were insensitive to width-to-thickness ratio and to cross-sectional area. Differences were observed in the values of total elongation but no definite trend could be established.

[redacted]

[redacted]

Photographs of an anodized grid pattern on the faces of the specimens made at various stages of axial strain permitted following of the movement of grid intersections to examine local strain patterns and homogeneities. Width strains were quite uniform across any particular position along the length of the specimen. Variations of local axial strain were definitely related to variations in thickness strains. Such variations occurred only in the immediate area of the fracture. The position of the neck could be detected immediately after yielding occurred, and the center of the neck moved with total strain if the neck formed near a shoulder. The studies confirm our previous conclusion that round tensile specimens must be used if quantitative strain anisotropy measurements are to be useful.

Comparison of irradiated and control anodized oxide films in situ on zirconium showed no detectable effects due to irradiation by fast neutrons to 9×10^{18} neutrons/cm^2. Reflectance measurements on air-formed and water-corrosion thin oxide films on zirconium showed that useful measurements of optical properties and film thickness could not be made on films thicker than about 1600 A for air oxidation and 3000 A for water corrosion.

A new electrical discharge machining apparatus has been constructed which permits accurate machining without distortion of selected crystallographic planes on single crystal specimens, and of special shapes such as spheres and tensile specimens from single crystals of zirconium.

A spherical single crystal of zone-refined zirconium has been used to examine the orientation dependence of oxidation rate in dry air at 350°C. The highest rate occurred on and near the basal plane, the $\{10\bar{1}0\}$ to $\{20\bar{2}1\}$ planes, and in a band sweeping from the $\{20\bar{2}1\}$ plane across the specimen to between the $\{11\bar{2}2\}$ and $\{11\bar{2}1\}$ planes. Only one run has been made to date, and the interference colors are a first-order gold and a first-order blue (estimated at 200 and 500 A thickness, respectively).

[redacted]

[redacted]

5. Irradiation Effects in Alloys and Structural Materials

In our study of radiation-enhanced diffusion in alloys, we have been investigating radiation-enhanced segregation in copper-nickel alloys. An analysis of previous neutron-irradiation experiments leads to the conclusion that the production of nucleation sites for the segregation reaction may be an important factor. To test this idea, an experiment is described, in which a Ni–40 wt % Cu sample was irradiated by 2 Mev electrons at liquid nitrogen temperature. Upon subsequent isochronal annealing, nearly the same behavior was observed as for neutron-irradiated samples.

In preparation for a study of radiation-enhanced diffusion in body-centered cubic alloys, resistivity measurements, at temperature and upon quenching, have been carried out on Fe–3.7 wt % Si samples. The quenching studies indicate a decrease in the quenched-in resistivity upon quenching from above 400°C.

Precipitation is another diffusion-controlled reaction of metallurgical importance. The effect of radiation on the precipitation of nitrides in alpha iron is being investigated by internal friction techniques. By using an in-reactor flexure pendulum, a fivefold increase in the rate of nitrogen precipitation was observed following low-temperature neutron irradiation. However, an electron irradiation, under comparable conditions of temperature and dose, produced no change in the aging kinetics. As a result, it is concluded that individual vacancies and interstitials do not act as nucleation sites for the precipitation of nitrides in alpha iron.

Stress relaxation experiments are likely to be helpful in the study of similar reactions in other body-centered cubic metals, such as vanadium, tantalum, and niobium. Modification to a torsion pendulum to permit sensitive stress relaxation measurements are described.

The theory of the dynamics of dislocation motion in iron is described. A stress relaxation technique is used to evaluate the stress dependence of dislocation velocity and the mobile dislocation density for sheet tensile samples of Ferrovac E iron in the carburized and decarburized conditions. It appears that dislocation generation is more difficult in

[redacted]

the decarburized samples. Also, an experiment on electron irradiated iron indicates significant changes in the stress dependence of the dislocation velocity. The dislocation dynamics is analyzed in terms of the classical motion of a particle in a viscous medium.

The first of a series of reactor experiments designed to determine the effect of dose rate on radiation hardening in Ferrovac E iron is completed and the results are described. The plans for the future experiments are discussed, and photographs of assembled irradiation capsules are shown. Experiments on the strain-rate dependence of plastic deformation have been performed on unirradiated round tensile specimens and the results are described in terms of the yield and flow stresses and the Lüders strain.

The effect of hydrogen on the mechanical properties of steel is discussed, and the minimum neutron flux necessary to produce hydrogen attack is calculated for a 1% Mn carbon steel. A series of experiments to determine the effect of gamma radiation on hydrogen permeability in type 304 stainless steel was conducted. Although it was thought that the apparent permeability might be changed due to the dissociation of molecular into atomic hydrogen in the gamma flux, the results were essentially negative. However, the observed diffusion coefficients agreed with an extrapolation to lower temperatures of values in the literature.

The status of the SM-1 pressure vessel surveillance program is given. Also, elevated-temperature irradiations of impact and tensile samples of commercial pressure vessel steel are described. Modifications have been made in the hot-cell equipment.

The preliminary design of a converter facility is completed for providing fission-spectrum neutrons in the Bulk Shielding Reactor. In the facility, reactor neutrons are thermalized in D_2O and then converted to fission neutrons in a converter tube containing ^{235}U. The facility is expected to operate above 30 kw and to provide a flux of at least 10^{12} neutrons cm^{-2} sec^{-1}.

A liquid-nitrogen-cooled cryostat for the Bulk Shielding Reactor is under construction. Gaseous helium, precooled by liquid nitrogen, is circulated about the experiment chamber.

[redacted]

[redacted]

[redacted]

PART I.

METALS AND CERAMICS DIVISION

[redacted]

[redacted]

[redacted]

[redacted]

1. FUEL ELEMENT DEVELOPMENT

G. M. Adamson, Jr.

The objective of the Fuel Element Development Program remains the development of new or improved fabrication techniques for both complete fuel elements and for fuel or cladding materials. We are studying a variety of materials for both uses, selected to include the more promising ones for use at temperatures over a wide range.

We are presently emphasizing vapor deposition as a fabrication technique. Our ultimate goal is the fabrication of a fuel element by a one-step fuel-conversion process followed by formation of an integral cladding, both using thermochemical deposition methods. To achieve this goal, separate fabrication efforts have been directed toward the preparation of UO_2 as the fuel material and refractory metals, such as molybdenum, tungsten, vanadium, and their alloys, as the cladding material.

Improvements in the fabrication of uranium carbide and uranium nitride fuels are being sought through the use of sintering aids. These aids must lower the sintering temperature without having deleterious effects on other properties and must be useful with commercially available powders.

With minor improvements, aluminum dispersion fuel systems should be capable of meeting the fuel requirements of research reactors for many years. A small program is directed at increasing the loadings and improving the efficiency of such dispersions.

Direct Thermochemical Conversion of UCl_4 to UO_2

F. H. Patterson W. C. Robinson C. F. Leitten, Jr.

Thermodynamic calculations were made to investigate the feasibility of direct conversion of UCl_4 to UO_2 by the chemical vapor deposition process. The first method considered was hydrolysis according to the following reaction:

$$UCl_4 + 2\ H_2O \rightleftharpoons UO_2 + 4\ HCl \quad . \qquad (1)$$

[redacted]

Since the compound $UOCl_2$ has been reported,[1] the above reaction was expected to proceed according to the following steps:

$$UCl_4 + H_2O \rightarrow UOCl_2 + 2\ HCl \quad , \tag{2}$$

$$UOCl_2 + H_2O \rightarrow UO_2 + 2\ HCl \quad . \tag{3}$$

The calculated free energy of reaction (1) was near zero in the temperature range considered desirable for deposition (600 to 800°C). The calculated free energy of reaction (2), which would constitute the initial step in the UF_6 hydrolysis was a large positive number (+20 kcal) in the 600 to 800°C range. This indicates that the hydrolysis reaction is not advantageous.

Another reaction route involves the initial reaction of UCl_4 with oxygen and subsequent reduction of the product of the oxidation with hydrogen. There is not sufficient data to complete thermodynamic calculations on the oxidation reaction, but it has been observed[2] at ORNL that U_3O_8 is produced from the reaction of UCl_4 vapor and oxygen at 600°C. This indicates that UO_2 can be produced by controlled reactions involving the initial oxidation of UCl_4 with oxygen and subsequent reduction of the reaction product with hydrogen if necessary.

Experimental facilities necessary for this investigation are nearing completion. Experimental work will be started during the following quarter.

Deposition of Uranium Compounds by Lithium Reduction of UF_6

W. C. Robinson C. F. Leitten, Jr.

Calculations have been made to explore the feasibility of the reduction of UF_6 with lithium. The proposed reaction is

$$UF_6(V) + 6\ Li\ (V) \rightleftharpoons U(s) + 6\ LiF\ (V) \quad . \tag{4}$$

---

[1]S. A. Sehchuhariev, I. V. Vasilkova, A. I. Efimou, and V. I. Kirgyasev, Zh. Neorgan. Khim. 1, 2272 (1956).

[2]T. A. Gens, Oak Ridge National Laboratory, private communication.

This process has been shown to be thermodynamically feasible. The reaction (4) is thermodynamically favored by low temperatures and high pressures, but both of these must be sacrificed in order to maintain the LiF as a vapor. The initial operating conditions have been chosen to be 1250°C and 20 torr. When the operating conditions for this reaction are optimized and good control of the flow rate of lithium vapor is established, CH_4 will be introduced into the entering gas streams in an effort to deposit uranium carbide.

The experimental facilities necessary to perform these reaction studies have been designed and are under construction.

Deposition of Refractory Metals

J. I. Federer C. F. Leitten, Jr.

We have continued to study the deposition of rhenium and have initiated a study on the deposition of molybdenum. In previous rhenium deposition studies, the actual ReF_6 flow rates were unknown due to metering difficulties.[3] For molybdenum deposition, the MoF_6 was metered with a specially calibrated glass flowmeter. Exclusion of traces of moisture is required to prevent reaction between MoF_6 and glass.

Rhenium deposition has been studied over the temperature range 500 to 700°C in search of the conditions required to prepare homogeneous deposits. In general, our results substantiate earlier results that indicated that nodular growth occurred at the inlet to the reaction zone under high deposition rate conditions, that is, high deposition temperatures or large excess of hydrogen. Conversely, a ductile coating 1 to 2 mils thick and 12 in. long was obtained at 600°C and at 10 torr with a H_2-to-ReF_6 ratio of 12. The metal recovery, however, was only 50%, indicating that high recoveries may have to be sacrificed for smooth, uniform deposits using the aforementioned deposition technique.

---

[3]J. I. Federer and C. F. Leitten, Jr., Fuels and Materials Development Program Quart. Progr. Rept. Sept. 30, 1964, ORNL-TM-960, p. 2.

Molybdenum deposition has been studied over the temperature range 600 to 900°C with a H_2-to-MoF_6 ratio of 40 and pressures of 10 and 100 torr. Some high-density, smooth deposits have been obtained, but additional experiments are required to maximize the process.

Deposition of Refractory Uranium Compounds

R. L. Heestand C. F. Leitten, Jr.

Modifications of the deposition apparatus for direct conversion of UF_6 to UO_2 have been completed during the last quarter. We installed a mass flowmeter to provide better control of UF_6 feed rates. Previously,[4] a borosilicate glass flowmeter was used which gave flow variations on the order of ±20% with changes in ambient temperature. Calibration tests are being made on the mass flowmeter to compare calculated flows with actual flow by recording UF_6 cylinder weight loss as a function of time. The addition of the mass flowmeter also eliminates several possible leak sites and should contribute to the overall integrity of the system. A new deposition furnace has also been added that increases the available deposition zone length to 20 in. In addition to giving additional sample length for evaluation, the total allowable feed rate for the system is increased.

We are continuing to study the effects of oxygen and hydrogen feed concentration on stoichiometry of the deposited UO_2. Previously, we reported[4] stoichiometry of the deposit could be varied by changing oxygen concentration. These experiments were carried out at a low UF_6 feed rate (20 cm^3/min) with other system variables held constant. However, in experiments where the gas ratios that previously gave $UO_{2.001}$ were increased proportionally to increase deposition rates, the oxygen-to-uranium ratio also increased to the range $UO_{2.078}$ to $UO_{2.134}$. Deposition rates were increased from 0.004 in./hr to 0.011 in./hr. These experiments indicate that stoichiometry of the deposit is a function of both the gas concentration and feed rate for a given system size.

---

[4]R. L. Heestand and C. F. Leitten, Jr., Fuels and Materials Development Program Quart. Progr. Rept. Dec. 31, 1964, ORNL-TM-1000, p. 2.

In the next period, the experiments to determine effects of feed gas composition on stoichiometry of the deposit will continue. Experiments directed toward producing submicron stoichiometric UO_2 powder will be resumed to produce sufficient amounts for chemical and physical property evaluation.

Deposition of Tungsten Alloys

J. I. Federer C. F. Leitten, Jr.

We reported the vapor deposition of tungsten-rhenium alloys by hydrogen reduction of WF_6 and ReF_6 in the temperature range 450 to 700°C last quarter.[5] In these experiments, the greater ease of reducing ReF_6 compared to WF_6 resulted in rhenium-rich deposits near the inlet to the reaction zone. A stationary hot zone and the equivalent of a stationary injector at the entrance to the hot zone were used in these experiments. An alternate arrangement that may alleviate the nonhomogeneity problem substitutes a moving hot zone of short length for the relatively long stationary hot zone. The desired alloy composition would be obtained by adjusting the gas mixture and the desired thickness would be obtained by regulating the rate of movement of the hot zone.

Several moving hot-zone experiments have been conducted in which an 8-in.-long furnace was moved along the length of the deposition tube by 1/4-in. increments every 15 min until a total movement of 4 to 5 in. was achieved. The conditions and results of these experiments are shown in Table 1.1.[1] The moving hot zone maintained a relatively high rhenium content throughout a greater length of deposit than has been possible previously, and appears to have potential for depositing homogeneous alloys. Metal recoveries varied from 36% at 600°C to 93% at 800°C. As the deposition temperature increased, the fraction of tungsten recovered also increased, and this recovery was reflected by the lower rhenium

---

[5]J. I. Federer and C. F. Leitten, Jr., Fuels and Materials Development Program Quart. Progr. Rept. Dec. 31, 1965, ORNL-TM-1000, p. 4.

Table 1.1. Summary of Tungsten-Rhenium Moving Hot-Zone Experiments[a]

Alloy Designation	Temperature (°C)	Metal Recovery (%)	Distance from Inlet (in.)	Rhenium Content (%)
WRe-26	600	36	2	33
			4	36
			6	30
			8	21
			10	9
WRe-27	700	80	2	24
			4	13
			6	12
			8	3
			10	1
WRe-28	800	93	2	16
			4	15
			6	12
			8	6
			10	11

[a]Feed rate, cm^3/min: H_2, 1500
WF_6, 60
ReF_6, 10

contents. In the deposit prepared at 800°C, the composition of the deposit near the inlet approached the metal composition of the reacting gases.

Since the moving hot zone in these experiments was 8 in. long, a range of compositions was always being deposited throughout the reaction zone.[5] Movement of the hot zone, therefore, resulted in deposition of layers of varying rhenium content. These layers were readily observed by metallographic examination. The grain structure within the layer was mostly columnar, although nodular growths (several columnar grains originating at a point and growing faster than the surrounding deposit) were also observed. No metallographic evidence for sigma phase was

found, but the evaluation is not complete. Layered deposits and corresponding nonhomogeneity in both the axial and radial directions cannot be completely eliminated in this technique, but can be minimized by using a much shorter hot zone. A high-frequency induction power supply is being adapted, therefore, to provide a movable hot zone of suitable length. A high-temperature homogenization anneal may also be required to decrease compositional variations.

Deposition of Fine-Grained Tungsten

J. I. Federer C. F. Leitten, Jr.

Vapor-deposited tungsten having a fine-grained rather than columnar structure has been reported.[6] Although the cause of this phenomenon is not known, the effect was tentatively attributed to a vanadium impurity in the WF_6. In another case, a fine-grained tungsten deposit occurred on a molybdenum substrate, suggesting that traces of molybdenum can refine the grain structure. Vanadium, molybdenum, and other solutes having a high affinity for interstitial impurities may deposit as discrete oxide or carbide particles that disturb the normally preferred growth patterns and promote the nucleation of new grains. Attempts to dope tungsten with vanadium and molybdenum in order to study the nature of grain refinement have continued. In these experiments, the first objective was simply to add the elements to tungsten.

The initial attempts to dope tungsten with vanadium consisted of separately metering VF_5, WF_6, and hydrogen into the deposition furnace. Then, a mixture containing about 600 ppm VF_5 in WF_6 was used. The conditions and recovery values for these deposition experiments are shown in Table 1.2.

In experiments WV-1 through -5, the first observed effect of VF_5 was a decrease in metal recoveries as compared to deposition of unalloyed tungsten under similar conditions. (Recovery values of 98% were obtained

---

[6]R. L. Heestand, J. I. Federer, and C. F. Leitten, Jr., Preparation and Evaluation of Vapor-Deposited Tungsten, ORNL-3662 (Aug. 1964).

[redacted]

Table 1.2. Conditions and Recovery Values for Tungsten-Vanadium Deposition Experiments

Experiment Number[a]	Temperature (°C)	Flow Rate, cm^3/min			Recovery (%)
		H_2	WF_6	VF_5	
WV-1	900	2000	50	8	75
-2	800	2000	50	9	70
-3	700	2000	50	5	0
-4	700	2000	50	3	55
-5	600	2000	50	3	2
-6	600	1500	50[b]		80
-7	700	1000	50[b]		97
-8	800	1000	50[b]		94
-9	800	1000	50[c]		85
-10	700	1000	50[c]		76
-11	600	1000	50[c]		75

[a]Pressure = 10 torr.

[b]WF_6-VF_5 mixture heated to 35°C.

[c]WF_6-VF_5 mixture heated to 50°C.

for tungsten deposition at 600°C with a H_2-to-WF_6 ratio of 25 and a pressure of 10 torr). A green-colored material, identified as VF_3 by x-ray diffraction, was dispersed throughout the deposits and coated the surface. Due to dispersion of VF_3 through the metal, an analysis of vanadium as a doping constituent could not be obtained. Metallographic examination of these deposits revealed mainly a columnar grain structure. The dispersed VF_3 phase caused disruptions in the columnar structure, but a fine-grained tungsten deposit was not obtained.

In the next three experiments, WV-6 through -8, the WF_6-VF_5 mixture was used. The mixture and transfer lines were heated to 35°C to promote vaporization of the less volatile VF_5. In experiments WV-9 through -11, the mixture and transfer lines were heated to the boiling point of VF_5, about 50°C. Again, the metal recoveries were lowered by the presence

[redacted]

of VF_5 in the reacting gases, especially when the mixture was heated to 50°C. The compound VF_3 was not observed on the surface of these deposits. Chemical analyses for vanadium content and metallographic examinations are being conducted. Preliminary analytic results indicate that low-level additions of vanadium (< 100 ppm) were achieved.

Deposition of tungsten on a molybdenum substrate was performed in an effort to reproduce the fine-grained structure that has been observed previously. The tungsten deposited on molybdenum foil at 600 and 700°C, with a H_2-to-WF_6 ratio of 50 and at a pressure of 10 torr. As before, the WF_6 contacted molybdenum foil in the entrance to the deposition furnace. The possibility exists that trace amounts of molybdenum enter the gas stream by reaction with WF_6 and subsequently deposit with tungsten. Metallographic examination, however, revealed no grain refinement in the deposits. The grain structure was columnar throughout the deposits, even at the tungsten-molybdenum interfaces. Analyses for molybdenum content are being obtained. Subsequent doping experiments will utilize a WF_6-MoF_6 mixture.

Under the assumption that grain refinement results from nucleation of new tungsten grains by solute atom compounds, such as oxides or carbides, the effect may be observed only when the deposits contain sufficient impurities to react with the solutes. Once methods are devised for doping tungsten with reactive solutes, methods of deliberately adding controlled amounts of normally undesired impurities will be considered.

Characterization of Al-U_3O_8 Fuel Dispersions

D. O. Hobson C. F. Leitten, Jr.

Characterization of a fuel dispersion is desirable from at least two standpoints. The first of these is to develop a method whereby one can predict the irradiation behavior of a fuel plate from a knowledge of the behavior of the fuel during the fabrication procedures. The second is to characterize the fabrication behavior of the fuel so that one can know what properties to specify when purchasing commercial fuel. We believe that an evaluation of the fragmentation and stringering

properties of U_3O_8 dispersed in aluminum, based on criteria such as oxide density, surface area, and fabrication procedures can provide data which, when related to subsequent irradiation testing, will afford a sound basis for predicting irradiation behavior.

It was the purpose of this study to find a suitable way to quantitatively evaluate fragmentation and stringering in the material under consideration and to propose a model of sorts that can be used to predict the fabrication behavior of similar fuel dispersions.

Samples of commercial powders were ordered from three vendors. The purchase order requested high-fired U_3O_8, depleted, with no further specifications. The as-received properties of the three oxides are listed in Table 1.3. The oxides are identified by the letters D, N, and S to allow the vendors to remain anonymous. Figure 1.1 shows the three oxides in the as-received condition, respectively.

Following previously developed ATR fabrication procedures,[7] each type oxide was powder metallurgically dispersed in type X8001 aluminum powder and roll bonded with type 6061 aluminum. After rolling, a longitudinal section was removed from the center portion of each plate and examined metallographically. Representative microstructures of the three commercial oxides in the as-fabricated condition are shown in Fig. 1.2. Since the fuel particles were highly fragmented, it was desirable to use a counting method that did not depend upon line or point count methods or upon random counting methods for the determination of fragmentation. A very simple expedient was used, namely the counting of every particle and every fragment in the field of view. The distinction between a small fragment of a large particle and an original fine particle was oftentimes difficult to determine and was solely dependent upon the judgment of the investigator. Employing this counting procedure yielded fragmentation ratio values for three different oxides as shown in Table 1.4 together with the data used to generate the ratios.

---

[7]D. O. Hobson, R. L. Heestand, and C. F. Leitten, Jr., Fabrication Development of U_3O_8-Aluminum Composite Fuel Plates for the Advanced Test Reactor, ORNL-3644 (July 1964).

Table 1.3. Properties of Commercial Powders of U_3O_8

Oxide	Sieve Cut	Analysis (%)	Density[a] (g/cm^3)	Surface Area[b] (m^2/g)	Uranium Analysis (%)
N	−80 +100	0.009	8.28	0.026	84.60
	−100 +140	21.932			
	−140 +200	33.859			
	−200 +270	21.766			
	−270 +325	15.198			
	−325	7.237			
S	−80 +100	0.187	8.26	0.058	84.72
	−100 +140	25.630			
	−140 +200	33.299			
	−200 +270	20.803			
	−270 +325	12.899			
	−325	7.182			
D	+100	0.005	8.28	0.107	82.89
	−100 +140	7.256			
	−140 +200	37.029			
	−200 +270	39.760			
	−270 +325	13.230			
	−325	2.700			

[a]Vacuum impregnation.

[b]BET krypton adsorption apparatus technique.

On the basis of this analysis, the S-type oxide showed a wider range in the fragmentation index between samples than either the D- or N-type oxides. In addition, the S oxide had the lowest density and also the highest amount of fragmentation of the three oxides tested. Both these factors relate to the initial condition of the oxide. The as-received powder was found to contain numerous cracks and to have an angular, almost acicular, shape. When this oxide was fabricated, each particle readily broke up into small fragments. The fragmentation

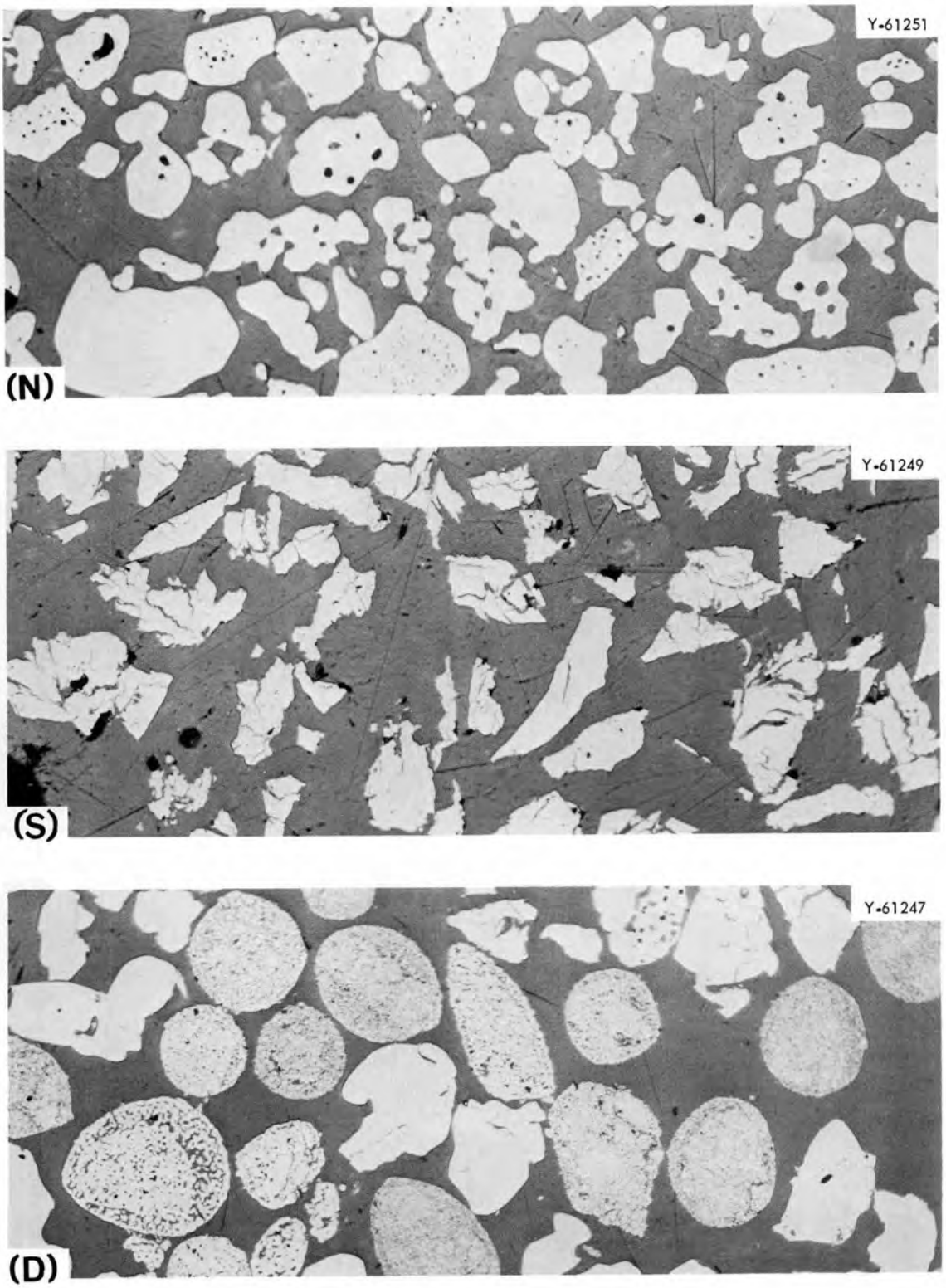

Fig. 1.1. Commercial Oxides N, S, and D in the As-Received Condition. As polished. 200×.

[redacted]

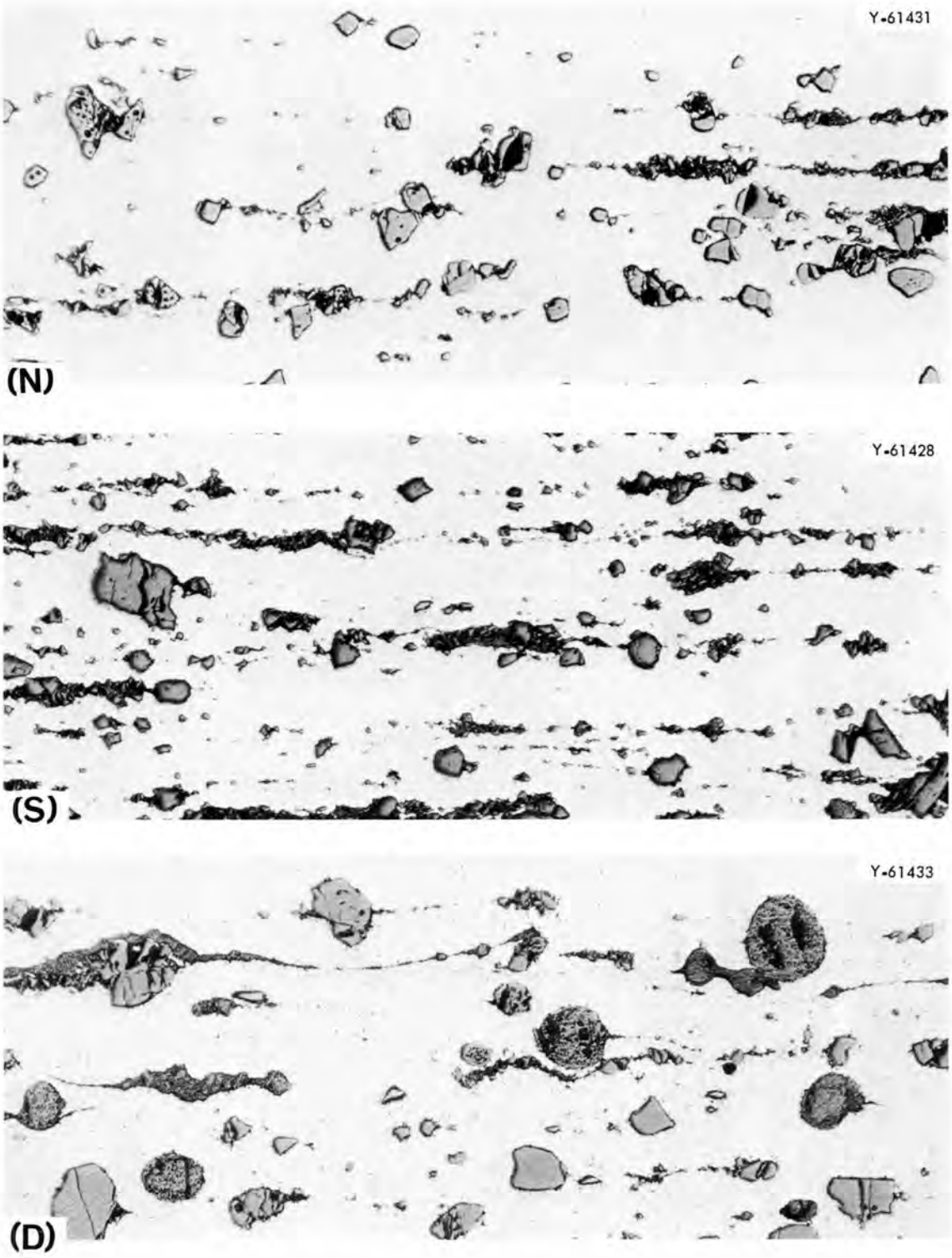

Fig. 1.2. Commercial Oxides N, S, and D in the As-Fabricated Condition. Hot, straight rolled 11.4:1; cold rolled 1.08:1; total reduction 12.3:1. As polished. 150X.

[redacted]

[redacted]

Table 1.4. Experimental Fragmentation Data on Commercial Oxides

Oxide	View Number	Number of Original Particles	Number of Fragments	Fragmentation Index	Average	Density (g/cm^3)
N	C-9-N (1)	450	3049	6.78		
	(11)	501	3384	6.75	6.90	8.28
	(21)	508	3359	6.61		
	(31)	554 (2013)	4092 (13884)	7.39		
S	C-7-S (1)	622	5812	9.34		
	(11)	561	5746	10.24	10.01	8.26
	(21)	556	5341	9.61		
	(31)	482 (2221)	5328 (22227)	11.05		
D	C-11-D (1)	491	2758	5.62		
	(11)	465	2561	5.51	5.86	8.28
	(21)	352	2252	6.40		
	(31)	511 (1819)	3095 (10666)	6.06		

values for the D oxide do not take into account the material contained in the stringered tails as shown in Fig. 1.2. This material was too finely divided to be resolved in the photographs. Further, these fine particles are not believed to be a manifestation of fragmentation but result from the removal of individual fines from the surface of many of the original oxide particles. The large surface area of this powder reflects the presence of these fines. Thus, the D oxide values represent an increase of the integrity of the particles, per se, seen in the matrix and not the material scoured from the surface during fabrication.

The fragmentation index for the N-type oxide was comparable to the D-type oxide in regard to density, but the degree of stringering in the N oxide is noticeably decreased. This effect we attribute to the low surface area of N-type oxide and the more spherical shape of the particles.

[redacted]

[redacted]

In summary, we have found that the fabrication behavior of oxide particles can be qualitatively predicted on the basis of the physical properties of the oxide and on the basis of particle shape. The degree of fragmentation increased with decreasing particle density. In addition, particle shape was observed to affect fragmentation in that spherical-type particles were much more likely to escape fragmentation during fabrication than particles having irregular shapes.

Based on the findings of this study, we recommend the specification of high density U_3O_8 (> 8.27 g/cm^3) with a spherical particle shape. We also recommend oxides having a low surface area (< 0.05 m^2/g) to eliminate the possibility of the tailing of fines from the surface of the particles.

[redacted]

2. NONDESTRUCTIVE TEST DEVELOPMENT

R. W. McClung

Our program is intended to develop new and improved methods of evaluating reactor materials and components. To achieve this we are studying various physical phenomena, developing instrumentation and other equipment, devising application techniques, and designing and fabricating reference standards. Among the methods being actively pursued are electromagnetics (with major emphasis on eddy currents), ultrasonics, and penetrating radiation. In addition to our programs oriented toward the development of methods, we are studying these and other methods for evaluation of problem materials and developing techniques for remote inspection.

Electromagnetic Test Methods

C. V. Dodd

We have continued research and development on electromagnetic phenomena on both an analytical and an empirical basis. As part of the program, we are studying the mathematical determination of impedance of an eddy-current coil and other electromagnetic field parameters as a function of coil dimensions, frequency, specimen conductivity and permeability, and coil-to-specimen spacing (lift-off). The relaxation techniques allow the solution of the electromagnetic boundary value problem on a digital computer. The differential equation for the field is approximated by finite difference terms. By making a number of correcting calculations, the value of the field can be made to converge to agreement with the differential equation at every point. The program is now being applied to study the shaping of the electromagnetic field and the eddy-current flow inside the material using ferrite. Figure 2.1 shows how equipotential contours of vector potential are shifted by the addition of a ferrite ring around a coil. Note how the contours are "squeezed" in toward the center line (axis) of the coil. Since the current density is proportional to the vector potential,

[redacted]

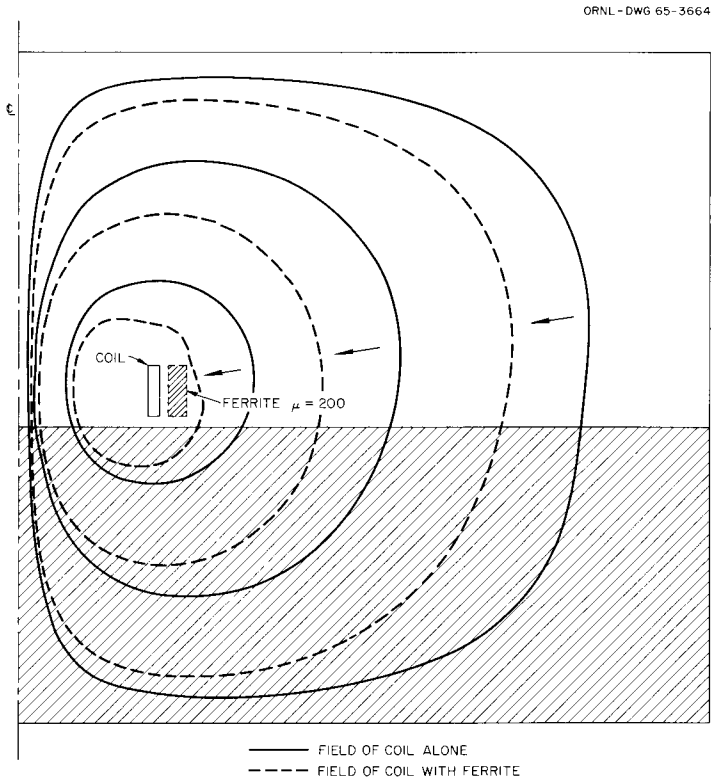

Fig. 2.1. Equipotential Contours of the Magnetic Field and the Eddy-Current Flow Using a Ferrite Ring Around the Core.

we can also see the change in current flow in the metal. Other shapes of coils and ferrites are being tried to obtain an optimum focusing of the currents inside the metal.

We are continuing development on the phase-sensitive eddy-current instrument. Harmonic distortion is one of the factors limiting the sensitivity of the instrument. The amplifiers and the oscillators of the system are being redesigned to minimize distortion, to increase the frequency range, and to permit use of inexpensive transistors. A power amplifier and video amplifiers have been designed with a 10-Mc bandwidth and 0.2% total harmonic distortion to 750 kc (the limit of our present distortion measuring equipment). The instrument previously had 1-, 2-, 5-, 10-, 20-, 50-, 100-, and 200-kc oscillators. We have designed 500-, 1000-, 2000-, and 5000-kc oscillators. These new oscillators should allow more sensitive inspections to be made of thin low-conductivity materials.

[redacted]

Ultrasonic Test Methods

K. V. Cook

Nonbond Studies

We have continued our studies on the behavior of ultrasound in thin sections with the principal effort being the detection of nonbonds in cladding structures. The through-transmission ultrasonic method has been used successfully to detect nonbonds in thin fuel plates by monitoring changes in transmitted intensity due to nonbonds. This same basic technique has been successfully applied to the evaluation of fuel tubes containing a cylindrical core of enriched UO_2 dispersed in stainless steel. We used a two-transducer through-transmission technique. A small probe that fit into the inner diameter of the fuel tube was used as the receiving transducer; the two crystals were aligned and fixed relative to each other; the combination moved longitudinally along the tube as it rotated and thus accomplished a helical scan. Figure 2.2 shows this system with the probe entering the tube bore. The helical wiper of a Mufax helical recorder was mechanically coupled to the rotary motion of the fuel tube to allow a "C" scan recording of nonbond areas. With this synchronization of fuel tube rotation and drum rotation, a straight line across the width of the recording paper represented the tube circumference. The spacing of these lines was determined by the speed at which the paper was pulled through the recorder and was proportional to the length of the fuel tubes. By using fast gating circuits, an electrical writing voltage was applied to the wire whenever a nonbond existed. Hence, positive writing was indicative of nonbonding and its location represented circumferential and longitudinal positions on the tube. We found that the attenuation variations inherent in the dispersion core were much less than that which would be expected from a nonbond as small as 1/16 in. in diameter.

Tubing Inspection

We are continuing to work on the problems encountered in tubing inspection. A major problem is the establishment of realistic ultrasonic notch standards for calibration. Since electrical discharge

[redacted]

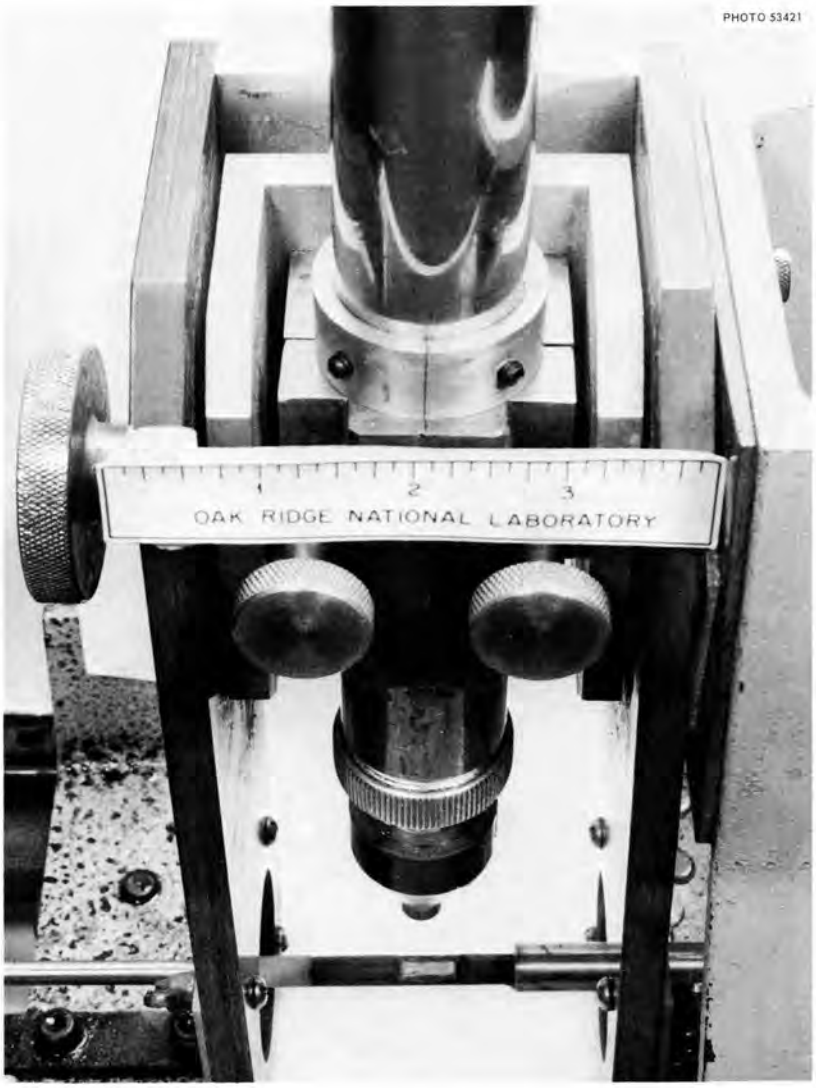

Fig. 2.2. Two-Transducer Through-Transmission System.

machining appears to be a reliable method for making both inner- and outer-surface notches, we are continuing our fabrication studies.[1] Calibration curves for machining of notches in types 347 and 304 stainless steel, molybdenum, Inconel, and Nb–1% Zr have been generated and

---

[1]K. V. Cook, Fuels and Materials Development Program Quart. Progr. Rept. Dec. 31, 1964, ORNL-TM-1000, pp. 39–41.

[redacted]

the latter is illustrated in Fig. 2.3. The nonzero intercept of the curve is due to the method of locating the zero tool feed position and, although it is small, the intercept will vary with the material. Further work is planned on different materials so that similar tool feed-to-notch depth curves can be established for each. Also, we hope to decrease the width of our notches until they more nearly resemble cracks.

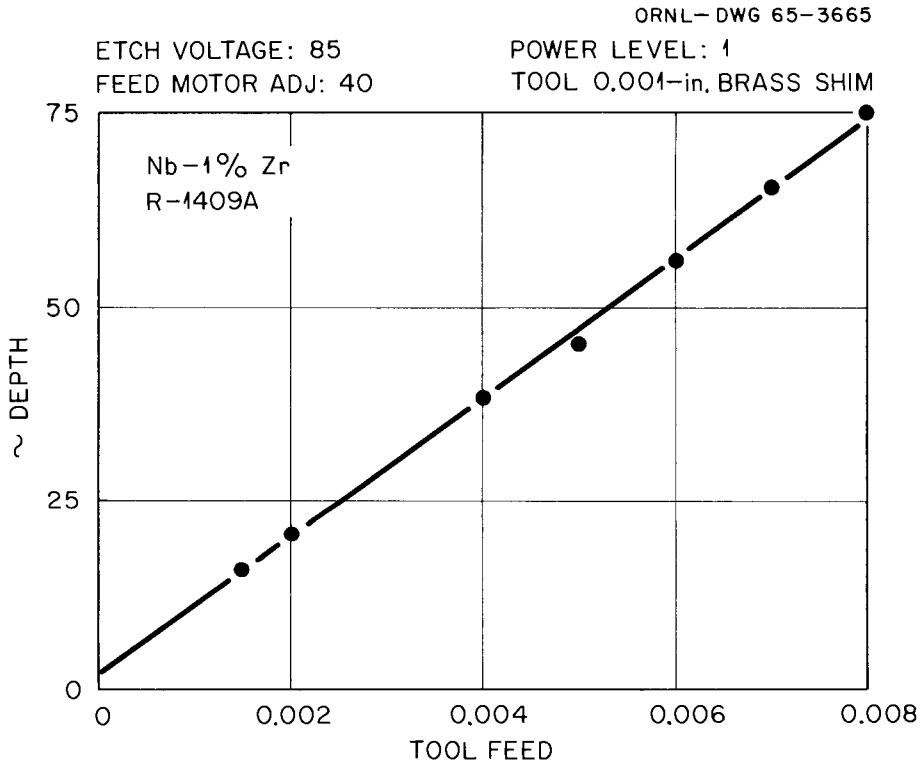

Fig. 2.3. Calibration Curve for Machining Notches in Nb-1% Zr Tubing.

[redacted]

Penetrating Radiation

Gamma Scintillation Gaging — B. E. Foster, S. D. Snyder

Photomultiplier Calibration System. — The photomultiplier calibration system[2] has been put into operation and has already proven useful. Recently we noticed a significant change in the operating levels of the detectors in both the fuel-rod scanner[2] and the fuel-plate homogeneity scanner.[3] The drift rate on these detectors had greatly increased and there was a decrease in sensitivity for a given change in radiation intensity. Subsequent evaluation of the detectors in the calibration chamber indicated poor spectral peak resolution and reduced overall gain. The photocathode was severely depleted on both detectors and the vacuum seal on one had developed a leak, allowing wetting of the crystal. Upon replacement of these detectors, the chamber was used to determine the proper operating potentials to optimize the performance of the new detectors.

Gaging Probes for Hollow Cylindrical Specimens. — We are in the preliminary stages of developing scintillation detector probes to be inserted into hollow cylindrical specimens for determination of fuel homogeneity by x-ray attenuation. These probes will consist of 1/4-in.-diam NaI(Tl) crystals coupled to Lucite light pipes of the same diameter. The other end of the light pipe is tapered to a 1-in. diameter for coupling to a 1-in.-diam photomultiplier tube. We have fabricated two light pipes, one 13 in. long that was machined to a 1/4-in. diameter over an 11 in. length; the other was made by gluing a 36-in. long, 1/4-in.-diam Lucite rod to a 1-in.-diam rod that was machine tapered to a 1/4-in. diameter over a 1 in. length. The glue, made by dissolving Lucite shavings in ethylene chloride, provides a joint with no change in refractive index. Both pipes were sprayed with a reflective paint, except on the coupling ends.

---

[2]B. E. Foster and S. D. Snyder, Fuels and Materials Development Program Quart. Progr. Rept. Dec. 31, 1964, ORNL-TM-1000, pp. 41–45.

[3]B. E. Foster, S. D. Snyder, and R. W. McClung, Continuous Scanning X-Ray Attenuation Technique for Determining Minute Inhomogeneities in Dispersion Core Fuel Plates, ORNL-3737 (Jan. 1965).

[redacted]

[redacted]

X-Ray Microscope — W. H. Bridges

Projection x-ray microradiography offers several advantages over contact microradiography. Contact microradiography is limited by the grain size of the recorded image and the light optics used to examine the image; whereas, with projection such limits are not imposed and the resolution is a direct function of the size of the x-ray source. Recently several electron-optical components became available. These are being modified and assembled into an x-ray projection system. The vacuum system has been tested and is satisfactory. The high-voltage electron gun supply has been assembled and testing is in progress.

Inspection Development of Problem Materials

K. V. Cook R. W. McClung

We have continued to work on nondestructive tests for unusual materials that are difficult to inspect and on new materials that have no evaluation history. This has included graphite and refractory metals including tantalum-, tungsten-, molybdenum-, nickel-, and niobium-base alloys.

Remote Inspection Development

K. V. Cook R. W. McClung

We have made a preliminary checkout of a remote scanning facility to be used to perform ultrasonic and eddy-current nondestructive testing in a hot cell.

The system has been modified to allow incremental transverse movements of the search tube in the manual mode of operation. Prior to this modification, the only way to make small quantitative well-controlled transverse movements on the search tube was in the automatic modes where each stepping operation is followed by a longitudinal movement of the search tube. With this modification the amount of stepping across a reference defect can be varied in increments as small as 0.001 in.

[redacted]

[redacted]

Another modification was made that allows an X-Y plotter to be used as a "C" scan recorder or as a slave device for indicating the location of the search tube in the scanning tank in the "hot cell." There is some hysteresis with change of direction with the major contributing factor being the gears in the mechanical system. Antibacklash nuts would cure much of this; however, we do not feel the expense of custom fabrication warrants their addition.

Other mechanical modifications are necessary before further check-out of the system can be accomplished.

[redacted]

3. SOLID REACTION STUDIES

T. S. Lundy

Our purpose is to provide information concerning solid-state reactions of importance in the development of materials for high-temperature application. We are emphasizing the study of mechanisms of these reactions by measuring diffusion rates in the solid state by various methods. In particular, we are studying the diffusion rates in various body-centered cubic refractory metals over wide ranges of temperatures.

Diffusion of ^{44}Ti in V–20% Ti

J. F. Murdock

Recent studies of radioisotopic diffusion in β-titanium and vanadium (ref. 1, 2) have revealed anomalous behavior in the variation of the diffusion coefficient with temperature. These anomalies, deviations from linearity in the Arrhenius-type plots, far exceed experimental errors and have not been explained mechanistically. This investigation is part of a continuing effort to understand this anomalous behavior, and atomic transport data are being determined in an alloy system of interest in the nuclear field.

The V–20% Ti alloy was electron-beam melted three times and drop-cast into a cylindrical mold. The castings were machined into specimens 5/8 in. in diameter and 1/2 in. long. Each specimen was given a homogenizing and grain growth anneal of 17 hr at 1500°C. This resulted in an average grain diameter of 1/8 to 1/4 in. One end of each specimen was mechanically polished and then chemically etched to remove the worked layer.

---

[1]J. F. Murdock, T. S. Lundy, and E. E. Stansbury, Acta Met. 12, 1033–39 (1964).

[2]T. S. Lundy and C. J. McHargue, Trans. Met. Soc. AIME 233(1), 243–44, (1965).

[redacted]

The HCl solution of ^{44}Ti was deposited drop-wise on polished surfaces and the liquid was evaporated. Diffusion anneals were performed in a split-tube tantalum resistance furnace at temperatures of 1200 to 1550°C in an atmosphere of 15 psig Ar. Lathe sectioning was used to determine the activity vs depth profiles from which the diffusion coefficients were calculated.

The diffusion coefficients are given below and summarized in Fig. 3.1. These data appear to follow the normal Arrhenius-type

Temperature (°C)	Diffusion Coefficient (cm^2/sec)
1545	9.41×10^{-9}
1500	6.52×10^{-9}
1454	3.43×10^{-9}
1400	2.18×10^{-9}
1352	1.02×10^{-9}
1300	5.31×10^{-10}
1250	2.88×10^{-10}
1200	1.52×10^{-10}

equation, $D = D_o \exp\left(-\frac{Q}{RT}\right)$; however, the temperature range is limited and must be extended to reach definite conclusions. This extension to lower temperatures (1050°C) is in progress. Higher temperatures (above 1550°C) are impractical because of severe preferential evaporation of the titanium from the alloy. An activation energy, Q, and a frequency factor, D_o, are not reported here because further data may alter the present interpretation.

In addition to extending the temperature range for this system, future experiments will span the vanadium-titanium phase diagram in the body-centered cubic phase and will include the diffusion of ^{48}V as well as ^{44}Ti.

[redacted]

[redacted]

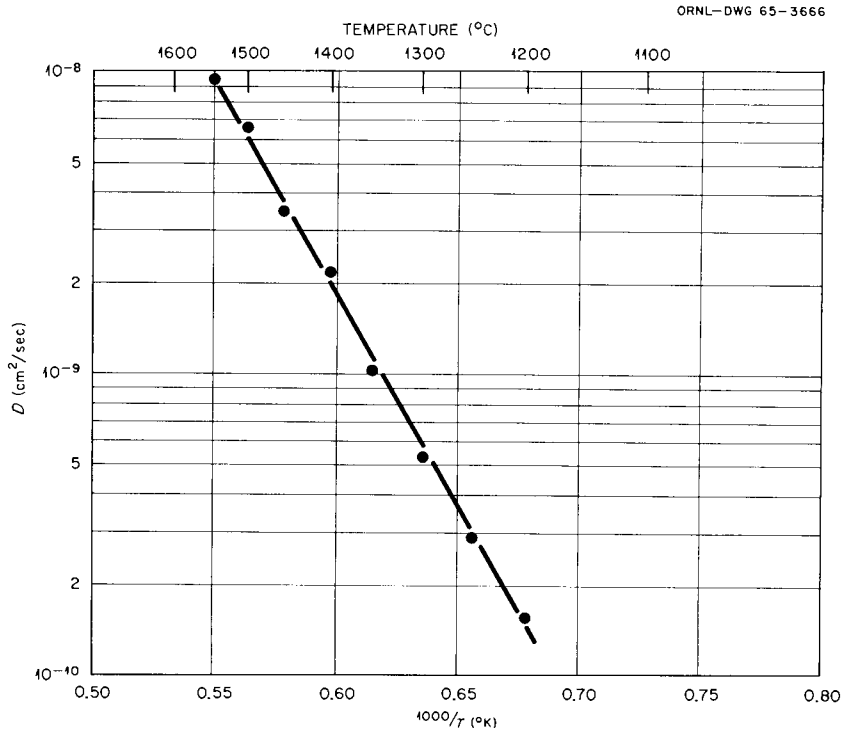

Fig. 3.1. Diffusion of Titanium-44 in V–20% Ti Alloy.

[redacted]

[redacted]

4. ZIRCONIUM METALLURGY

M. L. Picklesimer

We are conducting research along several lines on zirconium-base alloys of potential use as structural materials for water-cooled and/or -moderated reactor systems. The principal projects presently under way are: (1) studies of the physical metallurgy, consisting of transformation kinetics and morphologies, mechanical properties, phase diagrams, and heat-treatment response; (2) the development, evaluation, and utilization of preferred orientation and strain anisotropy in α-zirconium alloys during fabrication, and the utilization of yield stress anisotropy in increasing maximum permissible design stresses in structures; (3) the determination of the effects of composition, temperature, and environment on the oxidation-corrosion rates in the thin film stages of oxide growth; (4) a study of the effects of alloy composition and oxidation environment on the structural properties of thin oxide films *in situ*; and (5) investigation of stress reorientation of hydrides in Zircaloy-2.

Anisotropy in Zircaloy-2

P. L. Rittenhouse M. L. Picklesimer

The studies of the anisotropy of stress and strain in Zircaloy-2 conducted by this group in the past[1] were performed on round tensile specimens because preliminary studies had shown that the necessary information could not be obtained from sheet-type tensile specimens. One of the conclusions of those studies was a confirmation of the results of the preliminary studies. Another was that, qualitatively, the specimen geometry definitely influenced the strain pattern of the specimen, causing differences to be observed in elongation, yield strengths, and reductions of area. Quantitative data were not obtained

[1]P. L. Rittenhouse and M. L. Picklesimer, Metallurgy of Zircaloy-2 Part I: The Effects of Fabrication Variables on the Anisotropy of Mechanical Properties, ORNL-2944 (Oct. 1960); Part II: The Effects of Fabrication Variables on the Preferred Orientation and Anisotropy of Strain Behavior, ORNL-2948 (Jan. 1961).

[redacted]

at that time, and questions have been asked as to how the specimen geometry affected the test results in materials as anisotropic as Zircaloy-2. In addition, many of the materials to be tested are available only in thin sheet so that round tensile specimens cannot be readily made or tested. We have felt obligated to examine such effects, since we have been the major proponents of using round specimens for obtaining quantitative data on anisotropy.

Rolling and transverse direction sheet-type tensile specimens were made of very strongly textured (basal poles parallel to the normal direction) 1/8-in.-thick Zircaloy-2 sheet. Width-to-thickness ratios ranged from 10:1 to 0.6:1. All specimens were vacuum annealed at 650°C after machining. A square grid of lines, 0.050 in. apart, was applied by anodizing (using Kodak Photo Resist as a mask) over the entire reduced section of the specimen and well onto at least one grip section. The specimens were tested at a head rate of 0.1 in./min in an Instron Tensile Machine. Polaroid transparencies were made of the grid pattern on each specimen as assembled in the tensile machine and after various degrees of strain during each test. In each group of three duplicate specimens, one was strained to maximum load and removed from the machine, one was strained past maximum load until the neck was well developed and removed, and the third was tested to fracture.

The conventional mechanical property data on the specimen series are presented in Table 4.1. The yield strengths in the rolling and transverse directions were low and almost identical in value, in agreement with the degree and type of texture known to be present in the material. A small but definite increase in yield strength with decreased cross-sectional area was observed, independent of the width-to-thickness ratio. Both the ultimate strength and the reduction in area seemed to have been relatively insensitive to the width-to-thickness ratio and to the cross-sectional area. The elongations at maximum load also seemed to be insensitive; no explanation can yet be given for the high values observed for the "C" specimens. Differences were observable in the values of total elongation but no definite trend could be determined.

Table 4.1. Mechanical Properties of Zircaloy-2 Sheet-Type Tensile Specimens

Group	Original Area (in.^{2})	Width-to-Thickness Ratio	Total Elongation[a] ($\Delta\ell/\ell_o$)		Elongation[b] ($\Delta\ell/\ell_o$) at Maximum Load		Yield Strength[b] (psi)		Tensile Strength[b] (psi)		Reduction in Area[a] (%)	
			RD	TD	RD	TD	RD	TD	RD	TD	RD	TD
							$\times 10^3$		$\times 10^3$			
A	0.025	10.0	0.260	0.260	0.114	0.114	45.4	48.5	58.1	56.6	54	57
C	0.025	2.5	0.261	0.293	0.134	0.128	45.1	49.3	58.4	57.8	57	57
B	0.012	5.0	0.232	0.240	0.117	0.114	47.2	50.4	58.8	57.9	53	55
D	0.012	1.25	0.237	0.280	0.107	0.112	46.8	51.2	59.5	58.7	55	58
E	0.006	0.62	0.140	0.168	0.103	0.103	48.4	51.4	58.4	57.9	52	60

[a]Data from a single specimen.

[b]Average of three specimens.

[redacted]

Similar conclusions cannot, however, be reached as to the effects of specimen geometry on strain and strain ratio anisotropies. The transparencies of the specimens were projected and the intersections of the enlarged grid patterns were marked off on tracing paper. The movement of these intersections during straining could then be followed by overlaying the sheets of tracing paper on a light box. A typical strain sequence is shown in Fig. 4.1 for three positions on a tensile specimen, one position being the center line of fracture, and the other two at the outer boundaries of the neck. Folding of such tracings about apparent center lines of pattern demonstrated the homogeneity of strain occurring except for those specimens in which the neck formed near one shoulder. In such specimens, the restraint of the shoulder was made evident by the asymmetry across the fracture.

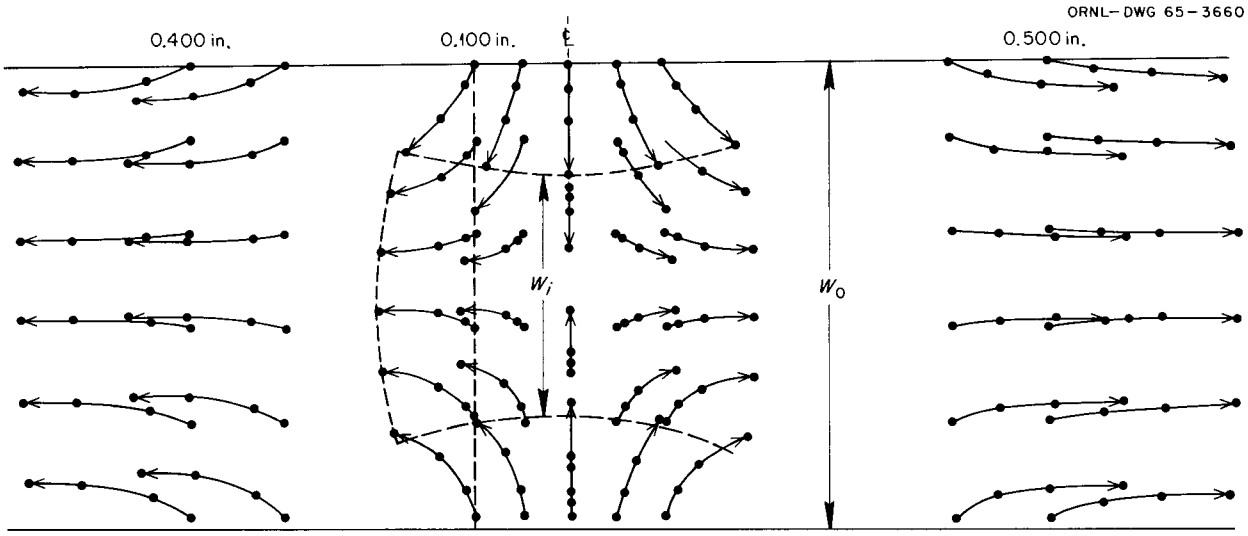

TRANSVERSE DIRECTION SPECIMEN AT −1
$W/T = 10$ W_0 = WIDTH OF UNSTRESSED SPECIMEN
W_i = WIDTH AT POSITION i FOR FRACTURE SPECIMEN

Fig. 4.1. Movement of Grid Points During Plastic Straining in a Zircaloy-2 Sheet Tensile Specimen.

[redacted]

Measurements were also made of the width strains, both micro and average, along the length of the specimen from the fracture towards each shoulder. At any point along the length, the microwidth strains did not vary across the width of the specimen, within the precision of measurements (including measurement with a split-image eyepiece microscope). Thus, the differences in microlength strains observed across any width position reflect differences in microthickness strains. The bowing of the first line of grid points away from the fracture center, as shown in Fig. 4.1, is a typical example. Precise measurements of microwidth strains along each line of grid points indicated that the width strains were the same for all positions across the width. Therefore, the differences in length strains made obvious by the bowing of the lines are directly related to differences in thickness strains. Such behavior was found only in the immediate area of the fracture, all other positions showing thickness strains too small to measure.

Consideration of the geometry of plastic strains of each of the grid units shows that changes in a grid area on the face of the specimen are direct measures of the true thickness strains at that grid position. Planimeter measurements of the grid areas on the transparency projections showed that no changes had occurred from the original areas (within the precision of measurement) other than in the immediate region of the fracture. Thus, in these specimens, no thickness strains occurred except at the fracture.

One of the measures of strain anisotropy previously developed is that of the strain ratios (called $\underline{k}$ values), that is, the ratio of contractile strain to the axial tensile strain for each of the principal directions. The $\underline{k}$ values for the three principal directions can be used to completely describe the three-dimensional strain anisotropy for round tensile specimens, and, we believe, for structural applications. In the sheet-type tensile specimens of this study, only $\underline{k}$ values for the width strains can be calculated, since no experimental measurement could be made of the thickness strains. A plot of the strain ratio, or $\underline{k}$ value as a function of axial strain should be a straight line if it is a characteristic of the material, as was observed in round specimens. A typical plot for a sheet-type specimen is shown in Fig. 4.2

[redacted]

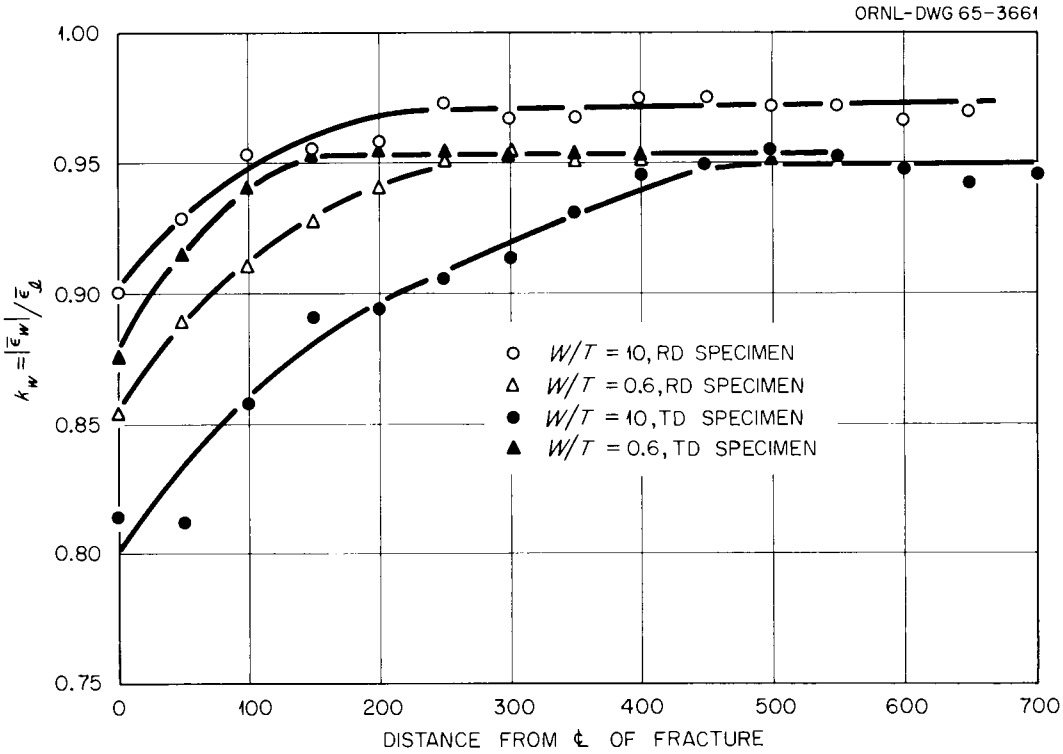

Fig. 4.2. Variation of Strain Ratios with Distance from Fracture in a Zircaloy-2 Sheet Tensile Specimen.

where it is observed that the strain ratio varies with total strain, particularly at the higher strains. Intercomparison of the data for the several specimens shows that the strain ratios also vary in no recognizable pattern with width-to-thickness ratio and specimen direction. Our earlier conclusion that strain ratios measured in the necked region of sheet-type tensile specimens cannot be used to characterize and describe three-dimensional strain anisotropy of the material is verified. We propose to repeat a portion of this experiment with material of a different and not so severe texture to determine if small strains in sheet-type tensile specimens can be used to determine k values, independent of width-to-thickness ratios.

One of the most interesting observations made in this study is that the neck position could be detected at a strain just beyond yielding and was obvious by the time maximum load was reached, the point at which necking is generally assumed to begin. The total width strains as functions of distance from the center line of fracture are shown in Fig. 4.3

[redacted]

[redacted]

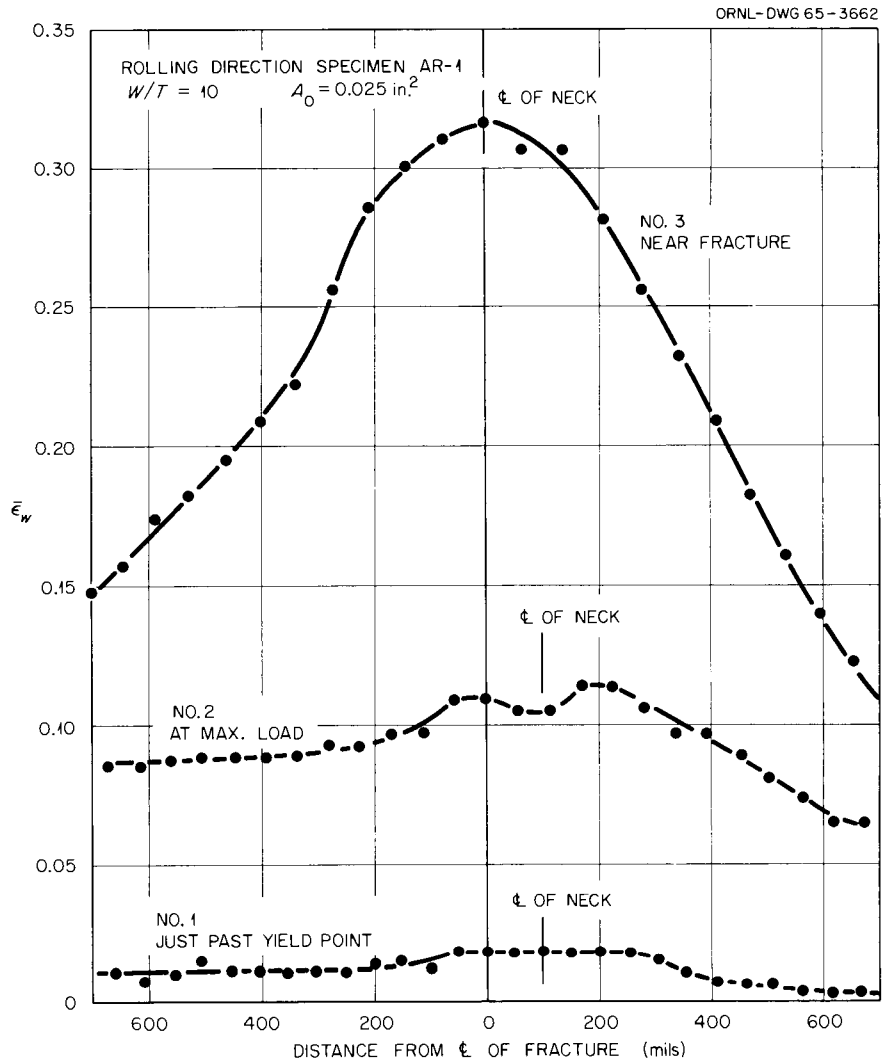

Fig. 4.3. Width Strains near the Neck of a Zircaloy-2 Sheet Tensile Specimen after Three Levels of Axial Straining.

[redacted]

for three conditions of test: (1) measured just after yielding; (2) measured at maximum load; and (3) measured at fracture. The curves in Fig. 4.3 and those for our many other specimens show that the center of the necked region can be transient during the early portions of plastic strain and that multiple necking definitely occurs. The asymmetry of curves 2 and 3 in Fig. 4.3 was caused by the proximity of the right-hand shoulder of the specimen during neck formation. The formation of the neck during the very early stages of strain will be investigated further.

Although some further studies will be made on sheet-type tensile specimens, our present experiences have strengthened our belief in the necessity and greater simplicity of using round tensile specimens when studying anisotropic materials.

Oxide Film Studies

J. C. Banter

Attempts were made to apply a modification of a technique recently reported by Wilkins[2] to the determination of the refractive indices of anodic oxide films *in situ* on zirconium. Analysis of the data collected from these measurements revealed that the assumption (on which the technique is based) that the film thickness is directly proportional to the anodizing voltage is spurious. Therefore, no absolute values for the refractive indices of the oxide films *in situ* were obtained.

The reflectance interference patterns measured as part of this technique were, however, compared to those measured for specimens anodized at the same voltages and then irradiated to a fast neutron dose of about 9×10^{18} neutrons/cm^2 in the ORR. No differences were observed between the interference patterns for the irradiated and unirradiated films, indicating no detectable changes in the indices of refraction had occurred with irradiation by neutrons. Such a change would have been

---

[2]N. J. M. Wilkins, "Optical Measurements of Oxide Films on Zirconium in the Range of Wavelengths from 2000 A to 2.5 μ," *Corrosion Sci.* **5**, 3 (1965).

expected if the irradiation had produced defects in the oxide film. It is possible that too few defects were produced to cause a detectable change in the refractive indices with the technique used.

Experiments are now in progress to measure the effects, if any, of the irradiation on the rate of dissolution of the oxide film into the base metal upon vacuum annealing the specimens at high temperatures.

Reflectance measurements made on air-formed and water-corrosion films indicate that the optical absorption of the films is so great that useful measurements cannot be made on air-formed films thicker than about 1600 A and on water-formed films thicker than about 3000 A. Such absorption must be due to a defect structure but the absorption observed occurs over such a broad wavelength range of the visible and ultraviolet regions that the types of defects cannot yet be determined.

Preparation of Single Crystals of Zirconium and Zirconium Alloys

J. C. Wilson

An electron-beam furnace for annealing specimens of zirconium and its alloys at pressures less than 1×10^{-8} torr has been built. The furnace will be used primarily for removing the last traces of hydrogen from specimens annealed for long times in an argon furnace in which some hydrogen pickup has always occurred.

A new electrical discharge machining apparatus has been completed. This machine allows us to cut crystal faces in single crystals to accurate orientations without deformation of the specimens, and micrometer adjustments of positions allow precise machining of spheres and other special shapes. A topical report on this machine is in preparation.

Zone Refining of Zirconium

J. C. Wilson

The vacuum system of the zone-refining apparatus became contaminated with diffusion pump oil when a mechanical forepump failed. An automatic protection system was designed and installed to prevent recurrence. The system was also modified during the downtime for cleanup to increase

pumping speed, a larger vacuum chamber was installed to prevent wall overheating when zoning large specimens, and provisions were made for more complete baking and higher baking temperatures. Improved vacuums and pump-down speeds have been obtained. The system is now back in full operation.

A borrowed residual gas analyzer was used to determine the composition of the gases in the system during baking and operation. No traces of pump oil have been found with proper operation of the system (partial pressure sensitivity of 1×10^{-10} torr, system pressure 5×10^{-9} torr). Thus, the few parts per million of carbon pickup observed during zone refining of zirconium does not appear to come directly from the pump oil, as had been feared. The principal contaminants observed were water, carbon monoxide, and hydrogen. We are presently trying to find ways of reducing the amounts of these gases during operation.

Properties of High Purity Zirconium

J. C. Wilson

Using a spherical single crystal of zirconium, we have clearly shown some of the dependence of oxidation rates on crystallographic orientation. A spherical specimen was oxidized in dry air for 1 1/2 hr at 350°C. The appearance of interference colors was observed during oxidation, and the process stopped when the first-order blue interference color was observed. The pattern of first-order blue color on the specimen is shown in the stereographic triangle in Fig. 4.4 by the shaded bands. The remaining portions of the specimen were uniformly colored a golden yellow. The estimated film thicknesses are about 500 A for the blue and 200 A for the gold. Pemsler[3] attempted to obtain similar information in oxygen at 415°C and Wanklyn[4] has attempted such

[3]J. P. Pemsler, The Diffusion of Oxygen in Zirconium and Its Relation to Oxidation and Corrosion, NMI-1177 (1957).

[4]J. N. Wanklyn, "Recent Studies of the Growth and Breakdown of Oxide Films on Zirconium and Its Alloys," Am. Soc. Testing Mater. Spec. Tech. Publ. 368, 58–75 (1964).

[redacted]

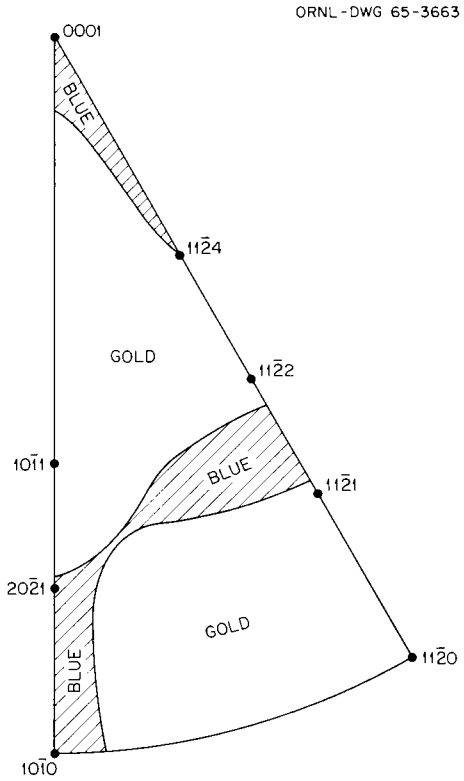

Fig. 4.4. Orientation Dependence of Oxidation in High-Purity Zirconium Single-Crystal Sphere. Cross-hatched areas represent orientations with film thickness roughly twice the other.

in 500°C steam. Both used large-grained polycrystalline specimens and the number of experimental observations available was insufficient to show the orientation dependence in the detail obtainable with a single-crystal sphere. Further studies on the spherical single crystals will be made to establish the effects of orientation on the kinetics of formation and growth of thin films of oxide in air, oxygen, water, and steam environments. We will also examine the anisotropy of oxygen diffusion by anodizing and estimating the dissolution rates at high temperatures from the color changes of the dissolving oxide films.

Studies on the recrystallization behavior of zone-refined zirconium have continued but have been hampered by a lack of good resolution of the microstructures at the start of recrystallization. We are developing electropolishing techniques and selective oxidation methods in attempts to resolve the structures.

[redacted]

[redacted]

[redacted]

[redacted]

PART II.

SOLID STATE DIVISION

[redacted]

[redacted]

[redacted]

5. IRRADIATION EFFECTS ON ALLOYS AND STRUCTURAL MATERIALS

D. S. Billington M. S. Wechsler

The Radiation Metallurgy Section of the Solid State Division at ORNL is engaged in research into the phenomena of radiation-enhanced diffusion, radiation hardening, and radiation embrittlement. These areas are closely interrelated. Our work on the face-centered cubic, copper-base alloys, copper-aluminum, and copper-nickel, has shown that when diffusion is enhanced by radiation a metastable alloy may revert to a more equilibrium atomic arrangement. In the case of copper-aluminum, the radiation-enhanced atomic rearrangement is believed to be short-range ordering, while for copper-nickel segregation is thought to be involved. These rearrangements may cause changes in mechanical properties. Some electron-bombardment experiments on copper-nickel alloy are described below, which indicate very similar effects as were observed upon neutron irradiation.

Because low-temperature brittleness is observed primarily in body-centered cubic metals and because radiation effects on the body-centered cubic metals have not been as widely investigated as for the face-centered cubic metals, the emphasis in our program is toward the body-centered cubic metals and alloys. To this end, some preliminary resistivity measurements have been made on iron-silicon alloys, at temperature and upon quenching. A decrease in resistivity upon quenching above 400°C suggests that it may be possible to observe radiation-enhanced atomic rearrangements in this alloy.

Another body-centered cubic alloy under investigation is iron-nitrogen. Here precipitation is the diffusion-controlled process influenced by radiation. As is described below, electron irradiation does not appear to accelerate the precipitation of nitrides, in contrast to the previously observed effect of neutron irradiation.

Since the strength of metals is largely controlled by the density and mobility of dislocations, a study of dislocation dynamics in iron is under way. A stress relaxation technique is being used to evaluate

the dependence of dislocation density and velocity in vacuum-melted iron of various purities and following various thermal and irradiation treatments. Similar experiments on other body-centered cubic metals are planned.

It is known that metals that exhibit low-temperature brittleness also show relatively large dependence of yield stress on temperature and strain rate. Therefore, experiments on the strain rate dependence of yielding in iron are under way.

The effect of neutron irradiation on the tensile properties of iron and steel is being studied by experiments in the ORR. Large increases in yield stress have been observed. Experiments are described below which are designed to evaluate the specific effect of dose rate on radiation hardening in iron. These experiments should have important implications for the use of structural metals in reactors under long-time, low-flux conditions.

The Charpy V-notch impact test is widely used to evaluate the susceptibility of engineering materials, particularly steels, to brittle fracture. A series of irradiations in the ORR have been performed at elevated temperatures on Charpy impact samples of a commercial pressure vessel steel. Calculations and a preliminary experiment dealing with hydrogen in steel have also been carried out and are described below.

Although the ORR will continue to serve as the major facility for the high exposure irradiations on engineering materials, unique and versatile facilities are being planned for the Bulk Shielding Reactor. These include a converter facility for fission spectrum irradiations and a cryostat for irradiations at liquid nitrogen temperature.

Low-Temperature Electron Irradiation of a Copper-Nickel Alloy

J. M. Williams B. C. Kelley M. S. Wechsler

In a previous report[1] the effect of low-temperature (−180°C) neutron irradiation upon a number of copper-nickel alloys was presented. It was found that the low-temperature bombardment produced little change in the electrical resistivity of the alloys, but large decreases in the resistivity were observed upon subsequent isochronal annealing up to 250°C. The magnitude of the decrease was largest in the Ni–40 wt % Cu alloy (about 1 μohm-cm). Recovery of the decrease takes place between 350 and 400°C. As a result of an earlier investigation by Ryan, Pugh, and Smoluchowski,[2] the resistivity decrease was attributed to neutron-enhanced segregation of the alloy components. The neutron irradiation is considered to provide a mechanism whereby the degree of segregation demanded by thermodynamic equilibrium at the lower temperatures (< 350°C) may more nearly be achieved. The crystallographic properties of the segregated structure have not been determined.

There are two mechanisms whereby neutron irradiation might be expected to enhance segregation in the alloy: (1) enhancement of diffusion by radiation-produced point defects; (2) production of damage clusters or displacement spikes which might serve as nucleation sites. In considering the likelihood of the first mechansim, it is useful to calculate the number of point defects produced by the irradiation. In the previous report, it was stated that the samples received a three-week irradiation in hole 50 of the ORNL Graphite Reactor. The thermal neutron flux in this hole is about 6.3×10^{11} neutrons cm^{-2} sec^{-1} and the fast ($E > 0.7$ Mev) flux is about 6.5×10^{10} neutrons cm^{-2} sec^{-1}. Coltman *et al.*[3] have

---

[1] J. M. Williams, W. Schüle, B. C. Kelley, and M. S. Wechsler, "Annealing of Cu-Ni Alloys Following Neutron Irradiation, Quenching, and Deformation," Quarterly Progress Report: Irradiation Effects on Structural Materials, HW-83398, p. 10.1 (Aug. 15, 1964).

[2] F. M. Ryan, E. W. Pugh, and R. Smoluchowski, "Superparamagnetism, Nonrandomness and Irradiation Effects in Cu-Ni Alloys," Phys. Rev. 116, 1106 (1959).

[3] R. R. Coltman, Jr., C. E. Klabunde, D. L. McDonald, and J. K. Redman, "Reactor Damage in Pure Metals," J. Appl. Phys. 33, 3509 (1962).

measured the damage rate in pure copper at liquid helium temperatures at a nearby position in the reactor, where the thermal flux is 6×10^{11} neutrons cm^{-2} sec^{-1}. They found that the total damage rate was 2.9×10^{-5} μohm cm hr^{-1} of which 0.57×10^{-5} μohm cm hr^{-1} was due to thermal neutrons and the rest was due to fast neutrons. Thermal neutron damage is caused by recoiling nuclei which have undergone (n,γ) reactions. Assuming the damage contributes a resistivity of 2 μohm-cm per atomic percent interstitial-vacancy pairs, we find the above fast damage rate is 1.19×10^{-7}/hr, and the thermal damage rate is 0.20×10^{-7}/ hr. We will assume the fast damage rate in the Cu-Ni alloy is the same as that in pure copper, since the elastic scattering cross sections for copper and nickel are about equal. The thermal damage rate of the alloy will be different from that of pure copper, however, because the capture cross sections and gamma recoil energies are different in nickel and copper. Using the methods given by Holmes,[4] we find the thermal damage rate of the Ni–40 wt % Cu alloy is 0.48×10^{-7} atomic fraction pairs/hr. Thus, the total damage rate is 1.67×10^{-7} atomic fraction pairs/hr. In three weeks time we have about 8×10^{-5} atomic fraction of pairs produced. (The reactor is shut down for 8 hr each week.) It should be reemphasized that this figure is based upon damage rates measured at 4.2°K and is, therefore, probably an overestimate for damage retained after a −180°C bombardment.

Let us compare the atomic mobility contributed by these defects to that in the unirradiated material. Previously we described experiments[1] in which the resistivity was measured upon quenching from various temperatures. It was found that the lowest temperature for which any excess resistivity could be retained was 350°C. This suggests that 350°C is the lowest temperature at which self diffusion in the alloy is capable of maintaining the equilibrium atomic arrangement. Thus, it can be said that the production and annihilation of 8×10^{-5} fraction of radiation-produced defects below 250°C gives a much larger decrease than is

---

[4]D. K. Holmes, "Radiation Damage in Non-Fissionable Metals," p. 147 in The Interaction of Radiation with Solids, ed. by R. Strumane, J. Nihoul, R. Gevers, and S. Amelinckx, North-Holland Publishing Company, Amsterdam, Netherlands, 1964.

observed upon aging, say, 1 hr at 350°C. Let us calculate the number of atomic jumps that might occur in 1 hr at 350°C. The activation energy for diffusion is given as 1.7 ev by da Silva and Mehl,[5] and this number is supported by the work of Schüle and Kehrer.[6] The number of jumps may be calculated from

$$\Gamma = \Gamma_o e^{-Q/kT} \tag{1}$$

where Γ is the atomic jump rate (total number of vacancy jumps per second per atom), $\Gamma_o = 10^{14}$ sec^{-1}, Q = 1.7 ev and T = 350°C = 623°K. The number of jumps, Γt, occurring in 1 hr is 5×10^3. In order for the 8×10^{-5} radiation-produced defects to provide this much atomic motion, each defect would have to make about 7×10^7 jumps, on the average, before annihilation. This number is not entirely unrealistic, but it seems rather high in view of the fact that we are considering 8×10^{-5} interstitial-vacancy pairs, most of which could presumably annihilate by recombination with only about 10^5 jumps per defect. Furthermore, as indicated above, the 5×10^3 jumps at 350°C do not produce observable changes in the resistivity anyway. If the diffusion enhancement provided by the 8×10^{-5} defects is to produce observable effects, the density of segregation centers must be higher in the temperature range where the radiation annealing takes place than at 350°C in the annealed material. There could be two explanations for this:

1. The driving force for the reaction is greater at the lower temperature and therefore additional sites for nucleating the segregation process are effective.

2. Nucleation sites for the reaction are produced upon neutron irradiation.

---

[5]L. C. Correa da Silva and R. F. Mehl, "Interface and Marker Movements in Diffusion in Solid Solutions of Metals," Trans. AIME 191, 155 (1951).

[6]W. Schüle and H. P. Kehrer, "Investigations on Vacancies and Phase Separation in the Copper-Nickel System by Means of Electrical Resistance Studies," Z. Metallk. 52, 168 (1961).

[redacted]

It was decided to test the latter possibility by subjecting the material to electron irradiation. Since electron irradiation is thought to produce mostly randomly distributed interstitial-vacancy pairs and isolated point defects, it was expected that the likelihood of radiation-produced nucleation sites in the electron irradiated material would be considerably less than in the neutron irradiated material. Accordingly, a sample of the Ni–40 wt % Cu alloy was irradiated to a dose of 9×10^{17} electrons/cm^2 with 2 Mev electrons at liquid nitrogen temperature. For a displacement cross section of 76.8 barns for the 2 Mev electrons,[7] the damage concentration is calculated as 7×10^{-5} pairs, a value very close to the neutron damage value. The resulting isochronal annealing curve is shown in Fig. 5.1. The annealing curve for the neutron irradiated specimen is shown for comparison. Except for the small decrease between −100 and 75°C in the neutron irradiated sample, the two curves are quite similar. This indicates that diffusion enhancement is probably the dominant mechanism in the radiation-enhanced segregation process. The density of segregation centers is probably greater during the segregation following irradiation than it is at 350°C, but this is a consequence of the fact that the segregation process is occurring at a lower temperature.

---

[7]O. S. Oen, Cross Sections for Atomic Displacements in Solids by Fast Electrons, ORNL-3813 (in press).

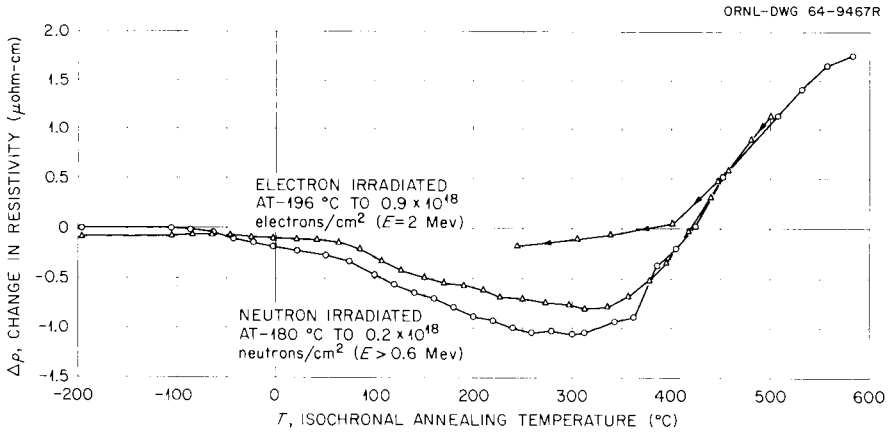

Fig. 5.1. Isochronal Annealing Curves for Ni–40 wt % Cu following Neutron Irradiation and Electron Irradiation at Less Than −180°C. The change in resistivity is taken with respect to the preirradiated value.

[redacted]

Resistivity Measurements in Fe–3.7 wt % Si

J. M. Williams M. S. Wechsler

The studies carried out on face-centered cubic alloys at the Oak Ridge National Laboratory and elsewhere over the past several years have amply demonstrated that irradiation accelerates the rate at which alloys can be equilibrated at lower temperatures.[8,9,10] It is a matter of both fundamental and practical interest to determine whether or not such effects take place in body-centered cubic metals, particularly iron and its alloys. Accordingly, a study of dilute iron-silicon alloys has been undertaken. The studies made thus far consist of laboratory resistivity measurements in preparation for irradiation experiments. Measurements of the resistivity as a function of temperature from −196 to 1050°C have been made for an Fe–3.7 wt % Si alloy. Also, the change in resistivity upon quenching from temperatures up to 850°C has been investigated.

A number of resistivity samples with 1-in. gage lengths were cut from an 0.008-in.-thick foil of Fe–3.7 wt % Si. The samples were annealed 2 hr at 1000°C and cooled at 50°C/hr to 400°C followed by a 25°C/hr cool to room temperature.

For the at-temperature measurements, a sample was mounted in a Lavite holder with thermocouples spot-welded to the ends of the sample just outside the potential probes. The resistance was first measured at liquid nitrogen temperature. Then the sample was placed in a vacuum furnace, and the resistivity was measured as a function of temperature up to 850°C (run A, Fig. 5.2). At this point, the temperature controller failed, and the sample was cooled to room temperature. After the controller was repaired, a new curve was obtained, which extended to 1050°C (run B, Fig. 5.2).

---

[8] J. M. Williams, W. Schüle, B. C. Kelley, and M. S. Wechsler, "Annealing of Cu-Ni Alloys Following Neutron Irradiation, Quenching, and Deformation," Quarterly Progress Report: Irradiation Effects on Structural Materials, HW-83398, p. 10.1 (Aug. 15, 1964).

[9] M. S. Wechsler and R. H. Kernohan, "The Effect of Radiation Diffusion Controlled Reactions in Copper-Base Alloys," p. 81 in Radiation Damage in Solids, International Atomic Energy Agency, Vienna, 1962.

[10] G. J. Dienes and A. C. Damask, "Radiation Enhanced Diffusion in Solids," J. Appl. Phys. 29, 1713 (1958).

[redacted]

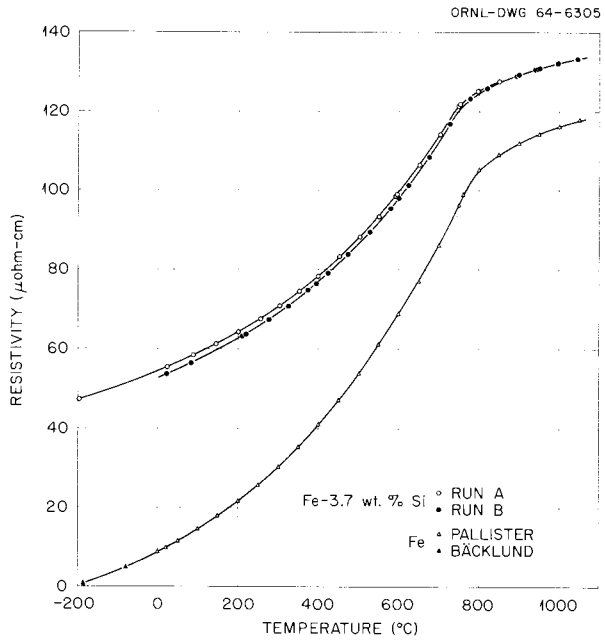

Fig. 5.2. Resistivity as a Function of Temperature for Iron and Fe–3.7 wt % Si.

The two curves showed roughly the same behavior, but they did not superimpose. Some earlier results for iron[11,12] are also shown in Fig. 5.2.

For the quenching experiments, the samples were suspended in a vertical vacuum furnace for 1 hr at the quenching temperature. Two quenching mediums were used, iced brine and diffusion pump oil. For the quenches into iced brine, the vacuum chamber was filled with helium, the bottom of the vacuum tube was opened, and the sample was dropped into a container filled with iced brine. For the quenches into diffusion pump oil, the oil was contained within the vacuum chamber, and the sample was quenched without interrupting the vacuum.

The results of the quenching experiments are shown in Fig. 5.3. The results of the iced-brine quenches were less reproducible than those for the oil quenches, as can be seen by the erratic behavior near 800°C

---

[11]D. R. Pallister, "The Specific Heat and Resistivity of High-Purity Iron up to 1250°C," J. Iron Steel Inst. (London) 161, 87 (1949).

[12]N. G. Bäcklund, "An Experimental Investigation of the Electrical and Thermal Conductivity of Iron and Some Dilute Iron Alloys at Temperature above 100°K," Phys. Chem. Solids 20, 1 (1961).

[redacted]

[redacted]

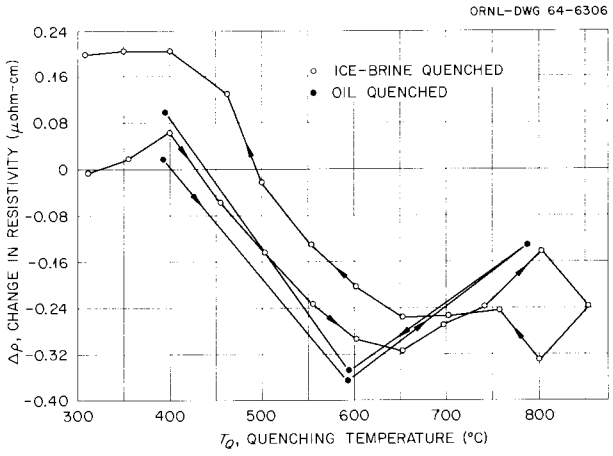

Fig. 5.3. Change in Resistivity vs Quenching Temperature for Fe–3.7 wt % Si. Measurements at –196°C.

and the lack of reversibility upon reducing the quenching temperature. The higher resistivity values upon decreasing the temperature are attributed to a coating of oxide, which was more severe for the iced-brine quenches than for the oil quenches. However, for both types of quenches there is a decided decrease in the resistivity upon quenching from above 400°C, which suggests a rearrangement of the iron and silicon atoms. Experiments will be performed to see if this rearrangement is enhanced by irradiation.

Precipitation of Nitrides in Electron Irradiated Iron

J. T. Stanley

Previously reported work[13] has shown that neutron irradiation markedly enhances the rate of removal of nitrogen from supersaturated solid solution in iron. We concluded that this effect was caused by an enhanced rate of precipitation of the metastable nitride, $Fe_{16}N_2$. A vacancy-nitrogen atom association of the type proposed by Damask and

---

[13]J. T. Stanley, "In-Reactor Internal Friction Measurements of Interstitial Rearrangements in BCC Metals," Quarterly Progress Report: Irradiation Effects on Reactor Structural Materials, HW-80794, p. 10.1 (Feb. 14, 1964).

[redacted]

co-workers[14] for the case of carbon in iron was eliminated as a possible explanation for the effect since not enough point defects were produced during the irradiation to trap a significant fraction of the nitrogen atoms. The enhanced precipitation is most certainly due to nucleation sites produced in the material during the irradiation since the rate of diffusion of nitrogen is not affected by radiation damage. The nitrogen atoms occupy interstitial positions in the lattice and so diffuse without the aid of vacancies. The fact that the temperature of the nitrogen internal friction peak did not change during irradiation shows that the nitrogen diffusion constant was unchanged during the irradiation.

In order to obtain a better understanding of the nature of the nucleation sites, an investigation into the effects of electron irradiation on precipitation of nitrides in iron was started. To date, one electron irradiation on nitrided iron has been carried out, and we believe the results are very significant for our understanding of the nature of the nucleation sites produced by neutron irradiation.

In this first electron irradiation, a specimen of the same type used for the neutron irradiation was irradiated with 2 Mev electrons at a temperature of about 0°C for 30 min and a current density of 2 $\mu a/cm^2$. After irradiation, the specimen was placed in the internal friction apparatus, and the aging of the internal friction peak at 65°C was studied. The irradiation dose was chosen so that the number of defects produced would correspond to the number produced by a one-day neutron irradiation in the graphite reactor, which corresponds to 3×10^{15} neutrons/cm^2 ($E > 0.6$ Mev). This neutron dose increased the rate of precipitation by a factor of 5. The irradiation temperature

---

[14]H. Wagonblast and A. C. Damask, "Kinetics of Carbon Precipitation in Irradiated Iron," Phys. Chem. Solids 23, 221 (1962); F. E. Fujita and A. C. Damask, "Kinetics of Carbon Precipitation in Irradiated Iron — II Electrical Resistivity Measurements," Acta Met. 12, 331 (1964); R. A. Arndt and A. C. Damask, "Kinetics of Carbon Precipitation in Irradiated Iron — III Calorimetry," Acta Met. 12, 341 (1964); H. Wagonblast, F. E. Fujita, and A. C. Damask, "Kinetics of Carbon Precipitation in Irradiated Iron — IV Electron Microscope Observations," Acta Met. 12, 347 (1964).

was chosen so that the nitrogen atoms would be immobile during the irradiation, but the defects would not. In this way it seemed that the concentration of defects would not become high enough to allow clustering of defects to occur.

The aging of the nitrogen internal friction peak for this sample before and after irradiation is shown in Fig. 5.4. There is no change in the aging kinetics of the electron irradiated sample. This is a most significant result since it shows that individual vacancies or interstitial iron atoms do not act as nucleation sites for the precipitation of nitrides.

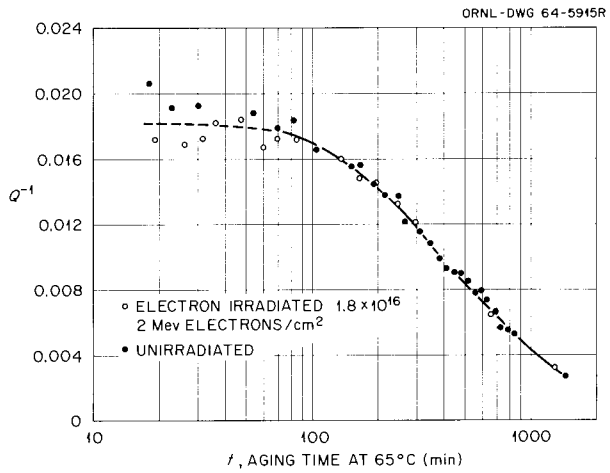

Fig. 5.4. Isothermal Aging of the Nitrogen Internal Friction Peak for an Electron Irradiated Specimen Vibrating in Flexure at 36 cps.

Electron irradiations should now be performed in which the specimen is held at liquid nitrogen temperatures during bombardment so that defects are immobile. Apparatus for this purpose has been constructed but is not yet completely tested.

Modification of Torsion Pendulum for Strain Relaxation Measurements

J. T. Stanley W. E. Brundage

Vanadium, tantalum, and niobium are body-centered cubic metals which exhibit Snoek-type internal friction peaks due to interstitial impurities.[15] The study of the interaction of radiation-produced point defects with interstitial impurities in these elements should be of considerable interest. However, the Snoek peaks in these materials occur at somewhat higher temperatures than the Snoek peaks in iron, and it is possible that any association of point defects with interstitial impurities might be disrupted by thermal energy below the temperature of the Snoek peak. This may explain why, in experiments on irradiated vanadium reported earlier,[14] there was little evidence for the trapping of vacancies at interstitial impurities similar to that reported by Damask and co-workers[14] for carbon in iron. An alternate possibility for the absence of an effect in vanadium is that the binding energy of a vacancy to an impurity atom is less than in iron, and therefore the impurity-vacancy complex is dissociated below the peak temperature.

The height of the Snoek internal friction peak can be studied at temperatures below the peak temperature by making strain relaxation measurements. The relationship between internal friction measurements and strain relaxation measurements can be pointed out by considering the equation for a standard linear solid[16]

$$\sigma + \tau_\epsilon \dot{\sigma} = M_R \left(\epsilon + \tau_\sigma \dot{\epsilon}\right) . \qquad (2)$$

This equation relates the stress, σ, and strain, ϵ, and their first time derivatives through three independent constants, τ_ϵ, τ_σ, and M_R, where τ_ϵ and τ_σ are the relaxation times at constant strain and stress,

---

[15] R. W. Powers and M. V. Doyle, "Diffusion of Interstitial Solutes in the Group V Transition Metals," J. Appl Phys. 30, 514 (1959).

[16] C. Zener, p. 43 in Elasticity and Anelasticity of Metals, University of Chicago Press, Chicago, Ill., 1948.

respectively, and M_R is the relaxed modulus. If a constant stress, σ_o, is applied to the solid at time t = o, then the strain relaxes to its equilibrium value, $\epsilon_f = \sigma_o/M_R$, with relaxation time τ_σ since under this condition Eq. (2) becomes

$$\sigma_o = M_R\,(\epsilon + \tau_\sigma \dot{\epsilon}) \ , \tag{3}$$

which has the solution

$$\epsilon = \sigma_o/M_R + (\epsilon_o - \sigma_o/M_R)e^{-t/\tau_\sigma} \ . \tag{4}$$

In Eq. (4) the quantity ϵ_o is the strain at time t = o, and we may replace this with σ_o/M_u, where M_u is the unrelaxed modulus. Equation (4) now becomes

$$\frac{\epsilon M_R}{\sigma_o} = 1 + \left(\frac{M_R - M_u}{M_u}\right) e^{-t/\tau_\sigma} \ . \tag{5}$$

From Eq. (5) we see that $(\epsilon_o - \epsilon_f)/\epsilon_f = (M_R - M_u)/M_u$.

For the case of internal friction measurement, periodic stresses and strains with frequency, ω, are considered. The solution to Eq. (2) then leads to the following expression for the internal friction

$$Q^{-1} = \frac{M_u - M_R}{\overline{M}} \frac{\omega\overline{\tau}}{1 + (\omega\overline{\tau})^2} \tag{6}$$

where $\overline{M}$ and $\overline{\tau}$ are the geometric means of M_u and M_R and of τ_σ and τ_ϵ , respectively. Comparing Eq. (5) and (6) we see that strain relaxation measurements measure $(M_R - M_u)/M_u$, which is very nearly twice the height of the internal friction peak occurring when $\omega = 1/\overline{\tau}$. However, because of the method of conducting the two different experiments, longer relaxation times are more easily measured by the stress relaxation technique. Since in the case of the Snoek internal friction peaks the relaxation time is an exponential function of temperature, longer relaxation times are found at lower temperatures.

The torsion pendulum in our laboratory has recently been modified so that strain relaxation measurements can be made with it. These modifications have been concerned primarily with increasing the sensitivity of the strain measurement and improving the isolation of the pendulum from mechanical vibrations. The improved sensitivity is

necessary for making strain relaxation measurements. The torsion pendulum shown in Figs. 5.5 and 5.6 has an optical lever of 4.8 m, and the position of the hairline on the scale can be read to 0.1 mm so that for a specimen 4 in. long and 0.030 in. in diameter, the strain can be read to 8×10^{-8}. With the use of the capacitance readout device, the strain reading can be improved by at least a factor of 10. This precision of strain measurement will allow us to measure strain relaxations corresponding to internal friction peak heights of 5×10^{-3} with an accuracy of better than 1%.

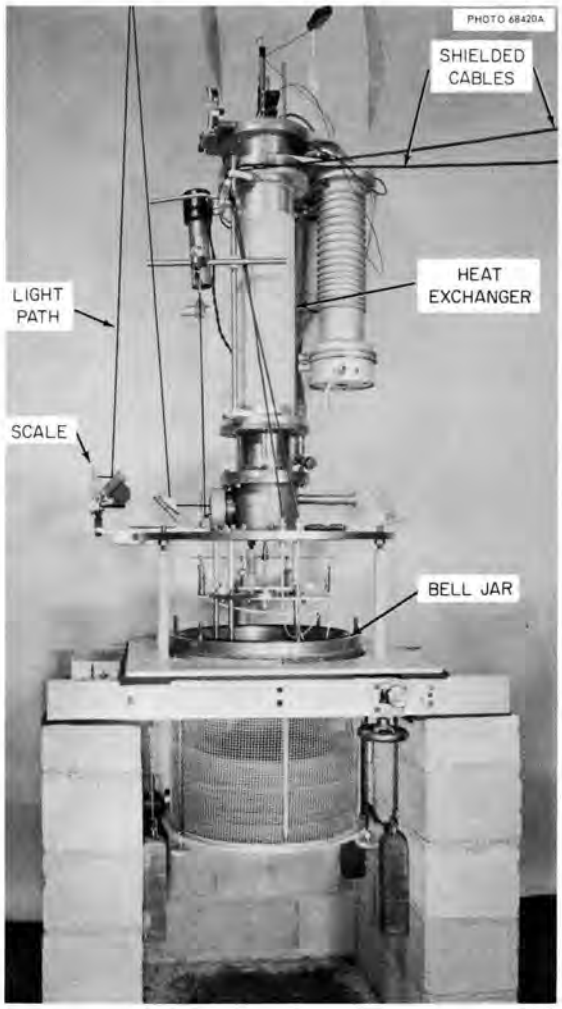

Fig. 5.5. Torsion Pendulum. The specimen used in the apparatus is a wire 4 in. long and 0.030 in. in diameter. It sits in the middle of the section labeled "heat exchanger." The specimen temperature can be lowered to about −170°C by circulating cold helium gas in the heat exchanger or raised to about 500°C by passing electrical current through a resistance winding on the heat exchanger.

[redacted]

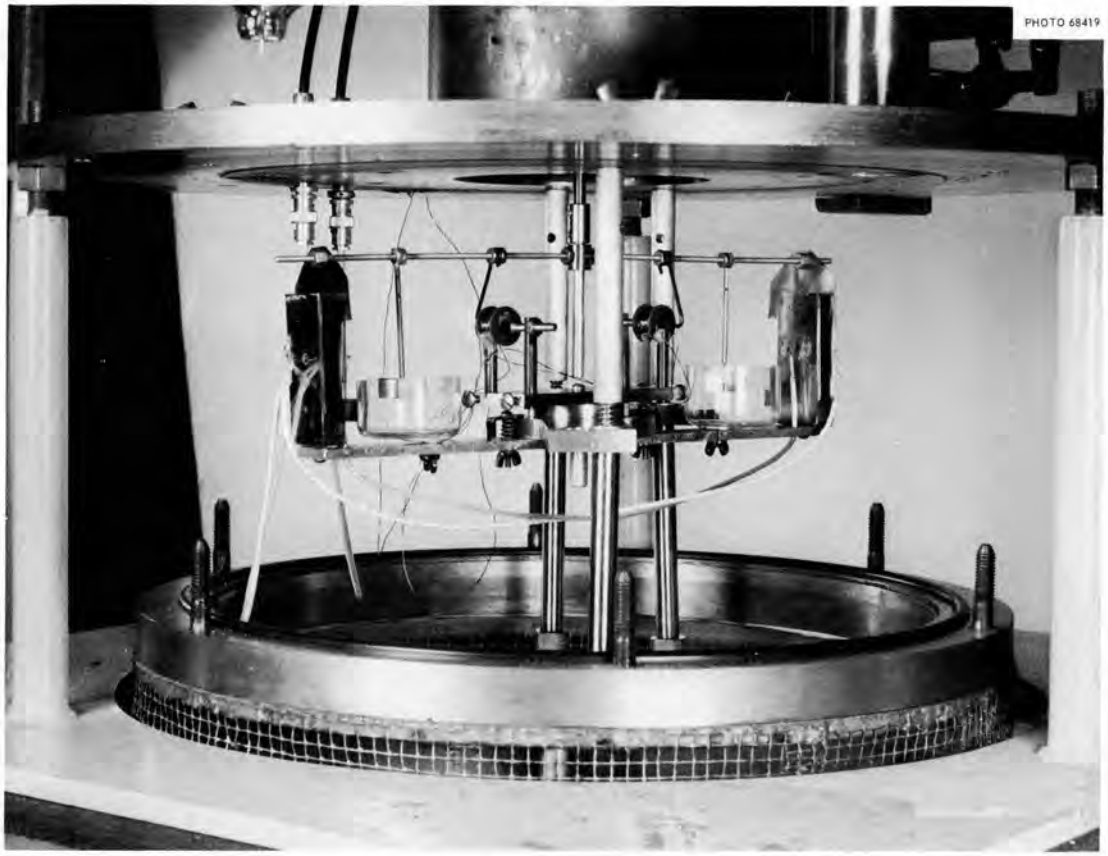

Fig. 5.6. Torsion Pendulum. Close-up of lower end of pendulum showing driving magnets, capacitance plates, and oil damping cups. The oil damping cups shown in the photograph damp out torsional oscillations, and are used only when making strain relaxation measurements. For internal friction measurements, these cups are removed.

Dislocation Dynamics in Iron

S. M. Ohr

Since Johnston and Gilman[17] successfully measured the velocity of dislocations in LiF by etch-pit techniques, the stress dependence of the dislocation velocity has been well established. Experimental data have often been represented by the empirical formula

$$v = (\sigma/\sigma_o)^m \quad , \tag{7}$$

[17]W. G. Johnston and J. J. Gilman, "Dislocation Velocities, Dislocation Densities, and Plastic Flow in LiF Crystals," J. Appl. Phys. 30, 129 (1959).

[redacted]

where v is the dislocation velocity, σ is the uniaxial tensile stress, σ_o is the stress corresponding to unit velocity and m is the index of the stress dependence of the velocity.

According to the dislocation model of plastic deformation,[18] the plastic strain rate imposed by the machine in a tensile test is given by

$$\dot{\epsilon}_p = 0.5\ b\ \rho\ v \quad , \tag{8}$$

where 0.5 is the orientation factor for tensile strain, b is the Burgers vector and ρ is the density of mobile dislocations. Thus, it is possible to express the flow stress in tension

$$\sigma = q\ \epsilon_p + \sigma_o\ (\dot{\epsilon}_p/0.5\ b\ \rho)^{1/m} \quad , \tag{9}$$

where q is the coefficient of linear work hardening. In this scheme, discontinuous yielding is a consequence of the stress dependence of the dislocation velocity and rapid dislocation multiplication. That is, the applied stress increases whenever there is an insufficient number of mobile dislocations, whereas the yield drop is a result of the rapid dislocation multiplication. It is expected that the yield and flow stresses depend solely on the parameters describing dislocation dynamics, namely $\dot{\epsilon}_p$, σ_o, ρ, m, and q.

In our effort to better understand the mechanism of radiation hardening in body-centered cubic metals, we have chosen to investigate systematically the effects of irradiation, as well as metallurgical variables, on these parameters. Existing data on iron[18] indicate that there are considerable scatters in the values of m and that the density of mobile dislocations, ρ, has never been measured. In iron the direct method of determining the dislocation velocity by etch-pit techniques has not been established. There are, however, several indirect methods of studying dislocation dynamics from tensile tests. We have found a

---

[18]G. P. Hahn, "A Model for Yielding with Special Reference to the Yield-Point Phenomena of Iron and Related BCC Metals," Acta Met. 10, 727 (1962).

stress relaxation technique[19] to be most suitable because the technique can be improved so that it presents a means of measuring the density of mobile dislocations during plastic deformation.

In the stress-relaxation technique a tensile sample is deformed to a certain amount of strain in an Instron machine, the cross-head motion is suddenly halted and the subsequent change in the applied stress is recorded continuously as a function of time (Fig. 5.7). When a tensile test is interrupted, the stress relaxes because the plastic flow continues as the dislocations gradually come to rest. Since the total strain rate is held to zero, the plastic strain rate is matched by an elastic strain rate, i.e.,

$$0 = \dot{\epsilon} = \dot{\epsilon}_e + \dot{\epsilon}_p$$

$$= \frac{1}{E}\frac{d\sigma}{dt} + 0.5\ b\ \rho\ (\sigma/\sigma_o)^m \quad , \qquad (10)$$

where E is the combined elastic modulus of the specimen and the machine.

[19]F. W. Noble and D. Hull, "Stress Dependence of Dislocation Velocity from Stress Relaxation Experiments," Acta Met. 12, 1089 (1964).

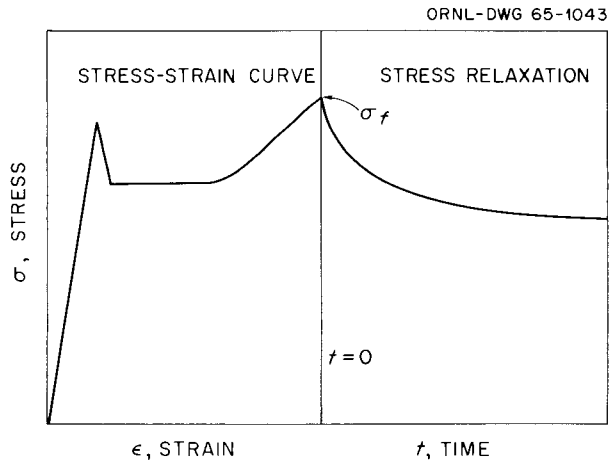

Fig. 5.7. Stress-Relaxation Experiment (Schematic).

The stress relaxation occurs according to the following differential equation

$$\frac{d\sigma}{dt} = -(0.5\ b\ E/\sigma_o^{\ m})\ \rho\ \sigma^m \quad . \tag{11}$$

In integrating Eq. (11), it was assumed previously that the density of mobile dislocation, ρ, remains constant during the stress relaxation.[19] We do not make such assumption here and instead integrate Eq. (11) by taking ρ to be a continuous function of time, i.e.,

$$\int_{\sigma_f}^{\sigma} \frac{d\sigma}{\sigma^m} = -A \int_0^t \rho(t)\ dt \quad , \tag{12}$$

where σ_f is the applied stress at $t = 0$ and $A = 0.5\ bE/\sigma_o^{\ m}$. From the mean-value theorem, the right-hand side of Eq. (12) can be replaced by the product of the average mobile dislocation density $\overline{\rho}$ and the time interval, t. Therefore, we get

$$\frac{1}{\sigma^{m-1}} - \frac{1}{\sigma_f^{\ m-1}} = (m - 1)\ A\ \overline{\rho}\ t \quad . \tag{13}$$

Since $\sigma_f^{\ m-1} \gg \sigma^{m-1}$, the second term on the left-hand side can be neglected. By taking logarithm of both sides, the solution of the differential equation may be written as

$$\log \sigma = \frac{\log t}{(1-m)} + \frac{1}{(1-m)} \log\ [0.5(m - 1)\ b\ E\ \overline{\rho}/\sigma_o^{\ m}] \quad . \tag{14}$$

When $\log \sigma$ is plotted against $\log t$, the value of m can be obtained from the slope and the intercept should yield the value of $\overline{\rho}/\sigma_o^{\ m}$. Figure 5.8 shows one such plot obtained from a Ferrovac E tensile sample. The results indicate that the stress relaxation is adequately represented by Eq. (14) and thus justify the model and the approximation employed in the analysis.

According to the etch-pit studies[17] in LiF and silicon iron,[20] the stress corresponding to unit velocity, σ_o, is proportional to the flow stress. The constant of proportionality, to the first approximation,

---

[20] D. F. Stein and J. R. Low, "Mobility of Edge Dislocations in Silicon-Iron Crystals," J. Appl. Phys. 31, 362 (1960).

[redacted]

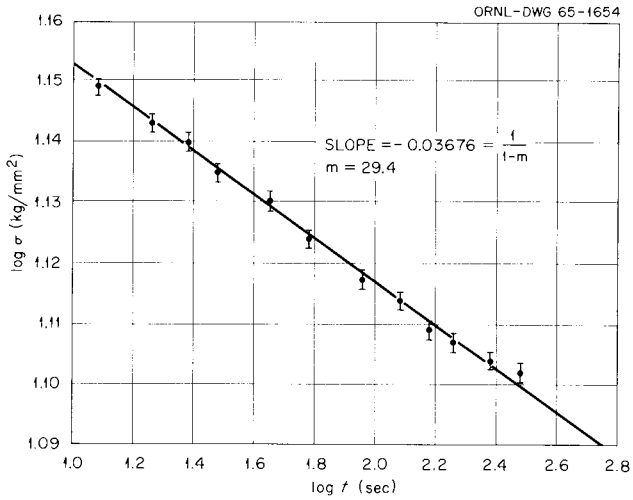

Fig. 5.8. Stress Relaxation of Ferrovac E Iron.

depends only on the material. In silicon iron, this is given by

$$\sigma_f = 0.77\ (\mathrm{cm/sec})^{1/m}\ \sigma_o \quad . \tag{15}$$

By accepting this correlation to be valid also in high-purity iron, the density of mobile dislocations can be evaluated from the intercept of a stress relaxation plot.

Figure 5.9 shows the results of the stress relaxation study performed on an 0.005-in.-thick tensile sample of Ferrovac E iron containing 40 ppm C by weight. The sample was annealed at 700°C for 2 hr, and this treatment resulted in the material having an average grain diameter of 20 μ. The deformation was carried out at room temperature and at a strain rate of 10^{-2}/min. After the sample was given a small amount of strain beyond the yield point, the tensile test was interrupted and the stress relaxation was measured. The sample was then deformed still further, and the relaxation measurement was repeated.

The results indicate that the exponent, m, for the stress dependence of the dislocation velocity remains nearly constant (m = 20) up to the Lüders strain, and then it increases rapidly with strain thereafter. Since σ_f/σ_o is taken as a constant that is less than unity throughout the test, it would imply that the dislocation velocity decreases with

[redacted]

[redacted]

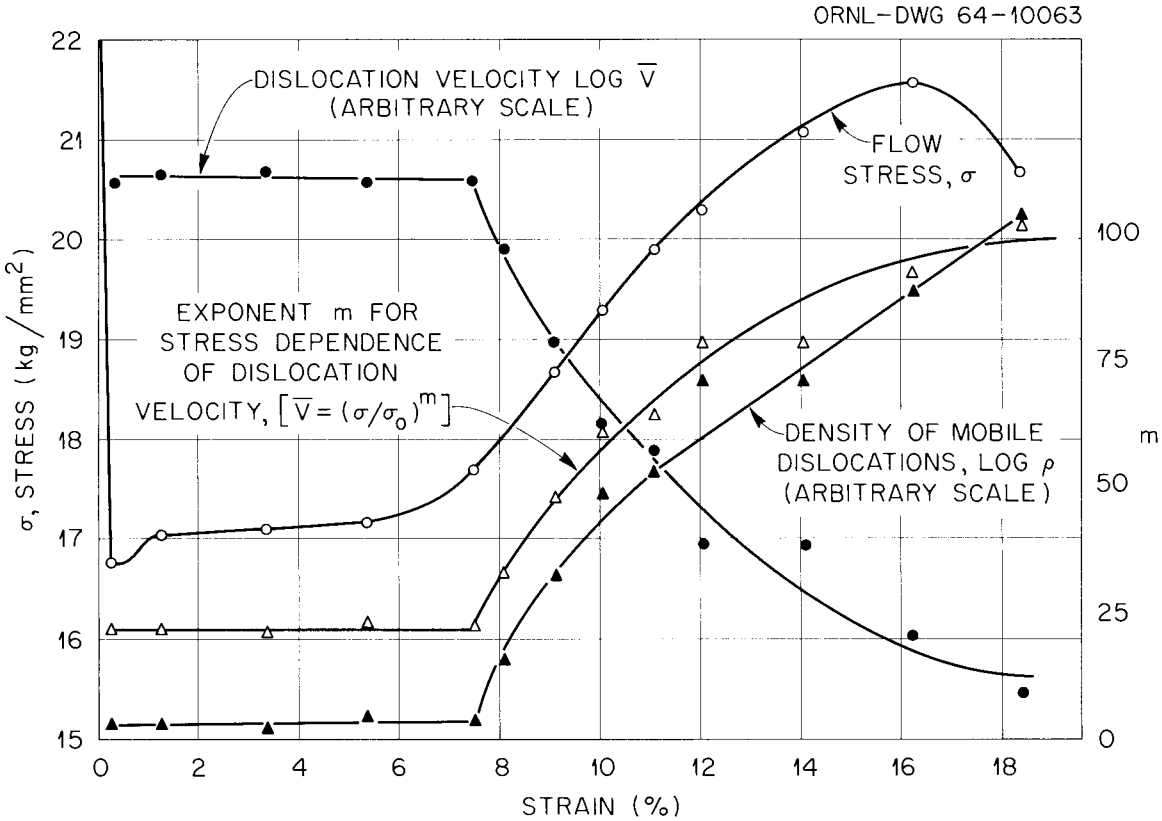

Fig. 5.9. Parameters Affecting Dislocation Dynamics in Ferrovac E Iron.

strain by approximately 10 orders of magnitude in the work hardening range of deformation. At the onset of plastic deformation, the density of mobile dislocations is found to be approximately $10^7/cm^2$, which is considered to be a reasonable estimate. The density increases rapidly with strain as the deformation is extended into the range of work hardening. Thus, as the metal work hardens an increasing number of mobile dislocations are generated, but they move at lower and lower velocities with increasing strain.

To investigate the effect of carbon content on the dynamical behavior of dislocations, a batch of Ferrovac E iron samples was decarburized at 800°C in an atmosphere of dry hydrogen which was purified through heated palladium-silver alloy. In the decarburized sample the initial value

[redacted]

of m is lowered to approximately 10, indicating that under an equivalent stress level the dislocations are moving at a velocity greater than that in the sample containing 40 ppm C. On the other hand, the density of mobile dislocations appears to have been lowered by many orders of magnitude. This would imply that, in the decarburized iron, the generation and the multiplication of dislocations are relatively slow processes. This may have resulted from the elimination of lattice inhomogeneities, such as inclusions, and also from the reduction of grain boundary areas caused by a rapid grain growth that is observed in the decarburized sample.

During the Lüders band propagation, we have found a break in the stress relaxation plot. This double stress relaxation may be taken as evidence for the presence of two species of dislocations which differ in mobility, density, and the resistance they encounter in the lattice. We have tentatively assigned to one of these two species of dislocations to be located at the band front and moving into the undeformed lattice and the other to be located behind the band front and moving in the slightly deformed lattice. A detailed analysis of the double stress relaxation phenomenon during the Lüders band propagation is in progress.

To study the effect of electron irradiation on the mechanical properties in terms of the dislocation dynamics, we have irradiated a tensile sample of Ferrovac E iron with 2 Mev electrons at a current density of 4 $\mu a/cm^2$ or 3×10^{13} electrons cm^{-2} sec^{-1} for a period of 4 hr, corresponding to a dose of 4×10^{17} electrons/cm^2. The temperature of irradiation was approximately 80°C. A preliminary result from the electron irradiated sample indicates that although the increase in the yield stress is limited to about 5%, the stress dependence of the dislocation velocity has changed significantly. The presence of two species of dislocations at the lower yield stress is also observed in the irradiated sample. It appears that only one of the two species of dislocations has undergone changes in its dynamical behavior upon irradiation.

We have attempted to interpret the physical significance of the stress dependence of the dislocation velocity. In this approach we consider a straight dislocation under a uniform applied stress which

[redacted]

is in the form of pure shear. The force per unit length of dislocation is $b\tau$ where b is Burgers vector and τ is the shear stress. The direction of the force is at right angles to the dislocation and this is taken as the direction of the dislocation motion. It is then assumed that the dislocation encounters a resistance of the lattice opposing its motion.

In analogy to the classical dynamics of a particle in a viscous medium, the equation of motion of a dislocation can be written as

$$M \frac{dv}{dt} + b\tau_r(v) = b\tau \quad , \tag{16}$$

where M is the effective mass per unit length of the dislocation and τ_r is the lattice friction force which is proportional to a power of the velocity. A particular solution may be obtained by setting $\frac{dv}{dt} = 0$, which describes the steady-state condition. Since the observed Eq. (7) should represent a uniform drift velocity attained by the dislocation, it may be taken as the particular solution of the equation of motion. Thus, we find that the lattice friction force should be of the form

$$\tau_r(v) = \tau_o \, v^{1/m} \quad , \tag{17}$$

and then Eq. 16 is written as

$$M \frac{dv}{dt} + b\tau_o \, v^{1/m} = b\tau \quad . \tag{18}$$

This may be taken as the equation of motion of a straight dislocation under the constant resolved shear stress τ.

Equation (18) may be integrated by the separation of the variables, i.e.,

$$t = \frac{M}{b} \int \frac{dv}{\tau - \tau_o v^{1/m}}$$

$$= - \frac{m \, M(\tau/\tau_o)^m}{b\tau} \left\{ \log \left[1 - v^{1/m}(\tau/\tau_o)\right] + \sum_{p=1}^{m-1} (\tau_o/\tau)^p \, v^{p/m}/p \right\} \quad . \tag{19}$$

[redacted]

From the boundary condition v = 0 when t = 0, the constant of integration is zero. By rearranging the terms

$$\left[1 - v^{1/m}(\tau/\tau_o)\right] \cdot \exp\sum_{p=1}^{m-1} v^{p/m}(\tau_o/\tau)^p/p = \exp\left[-b\tau(\tau_o/\tau)^m t/m\,M\right] \quad . \qquad (20)$$

This is the general expression relating the velocity of a dislocation with the uniform applied stress at any instant t. For a large t, the expression is simply reduced to the empirical formula of the stress dependence of the dislocation velocity. The relaxation time, taken by the dislocations in approaching the drift velocity, is given by

$$t_o = m\,M(\tau/\tau_o)^m/b\tau \quad , \qquad (21)$$

and its magnitude in a typical experiment is found to be of the order of 10^{-10} sec, if the effective mass per unit length of dislocation is approximated by the density of the crystal times the square of the Burgers vector.

We have shown that the dynamics of a dislocation in the crystal may be described by the motion of a particle of mass, M, in a viscous medium that exerts a friction force proportional to the $1/m^{th}$ power of the velocity. The parameter, m, therefore, represents the type of the lattice friction opposed to the dislocation motion, and the parameter σ_o indicates the magnitude of this friction. As the stress is applied to the lattice, the dislocations experience a period of rapid acceleration and then finally attain a drift velocity. This drift velocity is what one measures experimentally, for the transient state is expected to last only for a very short period of time.

Tensile Tests on Irradiated Iron and Iron Alloys

N. E. Hinkle N. K. Smith

It was previously reported[21] that a program to study the effect of neutron irradiation on the tensile properties of iron and iron-base alloys is under way. The irradiation of the first experiment assembly

[21] N. E. Hinkle, "Irradiation Effects on the Mechanical Properties of Iron and Iron Alloys," Fuels and Materials Development Program Quart. Progr. Rept. June 30, 1964, ORNL-TM-920, p. 113.

(ORR-56) has been completed. The experiment contained tensile samples of Ferrovac E of four grain sizes obtained by annealing at different temperatures in the α and γ phases. It was planned to analyze the results on the basis of the Cottrell-Petch equation

$$\sigma_{LY} = \sigma_o + k_y d^{-1/2} \tag{22}$$

which relates the lower yield stress, σ_{LY}, to the grain radius, d. In the original interpretation of this equation,[22,23] σ_o was identified as the friction stress inhibiting the motion of mobile dislocations, while k_y was proportional to the stress necessary to release a pinned dislocation from its locking atmosphere. The effect of radiation on the parameters σ_o and k_y has been a subject of some discussion in the literature.[24,25] Some studies have indicated that σ_o increases but k_y remains constant upon irradiation,[26,27,28] whereas other investigations have given changes in both parameters[29] or have found that Eq. (22) is no longer obeyed after irradiation.[30,31]

---

[22]N. J. Petch, J. Iron Steel Inst. (London) 174, 25 (1958).

[23]A. H. Cottrell, Trans. Met. Soc. AIME 212, 192 (1958).

[24]A. A. Johnson, N. Milasin, and F. N. Zein, p. 259 in Radiation Damage in Solids, Vol. I, International Atomic Energy Agency, Vienna, 1962.

[25]M. S. Wechsler, p. 296 in The Interaction of Radiation with Solids, North-Holland Publishing Company, Amsterdam, 1964.

[26]D. Hull and I. L. Mogford, Phil. Mag. 3, 1213 (1958).

[27]D. Hull, Acta Met. 9, 191 (1961).

[28]I. L. Mogford and D. Hull, J. Iron Steel Inst. (London) 201, 55 (1963).

[29]J. D. Campbell and J. Harding, p. 51 in Response to Metals at High Velocity Deformation, Interscience, New York, 1961.

[30]A. A. Johnson, Phil. Mag. 5, 413 (1960).

[31]A. S. Wronski and A. A. Johnson, Phil. Mag. 7, 1429 (1962).

The ORR-56 capsule was irradiated in a piggyback position in the pool of the ORR, extending from about 12 to 24 in. from the reactor face. Subsize round tensile samples were placed in vertical planes at four distances from the reactor face (see Fig. 6.25 of Ref. 21). The neutron flux was measured as a function of distance from the reactor face using cobalt, nickel, and iron monitors, and the results were presented previously (see Fig. 6.26 of Ref. 21). At three of the sample stations, the temperature was controlled at 40°C by placing the samples in hollows in half-round water-cooled coils. At the fourth station (second closest to reactor), electrical heaters were used to maintain the temperature at 260°C. Some interest is attached to the question of the relative effects of thermal neutrons and fast neutrons. The thermal neutrons may produce changes in tensile properties due to transmutations, (n,α) reactions with ^{10}B, or (n,γ) recoil events,[32] whereas the fast neutrons produce displacements chiefly as a result of atomic collisions. In the attempt to separate the effects of thermal and fast neutrons, certain samples were encased in 30-mil cadmium sheet which shields out the thermal neutrons. Also, in addition to the Ferrovac E iron samples, tensile specimens of Ferrovac 1020 steel and Commercial ASTM A-212, grade B, steel were included. However, thus far only the Ferrovac E samples have been tested, and only this material is discussed in what follows.

For the ORR-56 samples and the corresponding control samples, the heat treatments for the establishment of grain size were performed on blanks and the samples were machined out of the blanks subsequently. The results of tests on the control samples, carried out after the irradiation had started, are shown in Fig. 5.10 by the error limit symbols for $\phi = 0$. In this plot of σ_{LY} vs $d^{-1/2}$, it is seen that the yield stress values for these points lie significantly above the dashed line, which refers to previously reported data (see Fig. 6.20 of Ref. 21) for samples heat treated after machining. It is concluded from Fig. 5.10

---

[32] R. R. Coltman, Jr., C. E. Klabunde, D. L. McDonald, and J. K. Redman, J. Appl. Phys. 33, 3509 (1962).

[redacted]

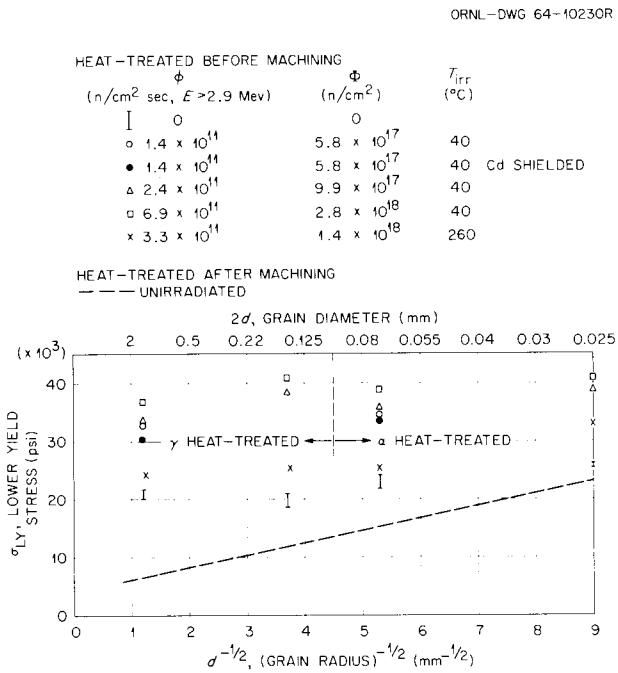

Fig. 5.10. Yield Stress vs (Grain Radius)$^{-1/2}$ for Ferrovac E Vacuum Annealed and Furnace Cooled (ORR-56). Strain rate, 0.02 min^{-1}; test temperature, 25°C.

that the samples for ORR-56 were cold-worked during the machining. This was confirmed by careful examination of additional samples machined under the same conditions as the original ones. It is observed in Fig. 5.10 that the increase in lower yield stress due to the cold work increases with increasing grain size or with decreasing yield stress of the as-heat-treated material. For the samples having a grain diameter of 0.025 mm corresponding to $d^{-1/2} = 9$ mm$^{-1/2}$, the cold work introduced by the machining was slight. Therefore, the results for samples of this grain size are not complicated appreciably by the effects of the machining.

The yield stress measurements for the irradiated Ferrovac E samples are also shown in Fig. 5.10. The percentage increase in yield stress due to the irradiation was about the same for each of the three irradiation doses at 40°C regardless of the amount of prior cold work. The cadmium shielding, used to decrease the thermal neutron flux incident on certain samples, appeared to reduce the increase in yield stress due

[redacted]

to the irradiation, but not by a large amount. The radiation hardening of the samples irradiated at 260°C was significantly less than for samples irradiated at 40°C. For the fine-grained samples ($d^{-1/2} = 9\ mm^{-1/2}$), the increase in yield stress for irradiation at 260°C was about one-half of the increase for irradiation at 40°C. However, for the coarser grain sizes where the effects of the prior cold working were evident, the 260°C irradiation may have caused some recovery of the cold-work increment to the yield stress in addition to the annealing during irradiation of some of the radiation hardening.

In the next series of experiments on Ferrovac E iron, the effect of dose rate will be investigated on samples of constant grain size irradiated at a constant temperature. Several experiment assemblies are scheduled for irradiation during the next six months, beginning in March 1965. Construction of six of these assemblies is nearing completion. The highest neutron flux, about 1.5×10^{13} neutrons cm^{-2} sec^{-1} (> 1 Mev), will be achieved in an ORR poolside position experiment shown in Fig. 5.11. The lowest neutron flux, about 4×10^{11} neutrons cm^{-2} sec^{-1} (> 1 Mev), will be obtained in a piggyback experiment behind the poolside experiment and about 21 in. from the reactor tank. A piggyback experiment is shown in Fig. 5.12. Neutron flux measurements will be made during the irradiations in order to choose the duration of the irradiations in a manner to obtain equal neutron dose for various neutron dose rates. The irradiation times being considered yield three dose levels in the range 3×10^{18} to 2×10^{19} neutrons/cm^2 (> 1 Mev). The tensile samples will be maintained at a fixed temperature between room temperature and 100°C.

The tensile test program will be designed to determine the effect of the neutron irradiations on the tensile parameters of lower yield stress, Lüders strain, work-hardening coefficient, and the strain-rate dependence of these parameters for one grain size having a $d^{-1/2}$ value of about 4 $mm^{-1/2}$. A few samples with a $d^{-1/2}$ value of about 11 $mm^{-1/2}$ have been included in some of these experiments to obtain some data about the grain size dependence after irradiation.

Strain rate has long been known to have a strong effect on yield and flow stresses of iron and steel at room temperature. Since the

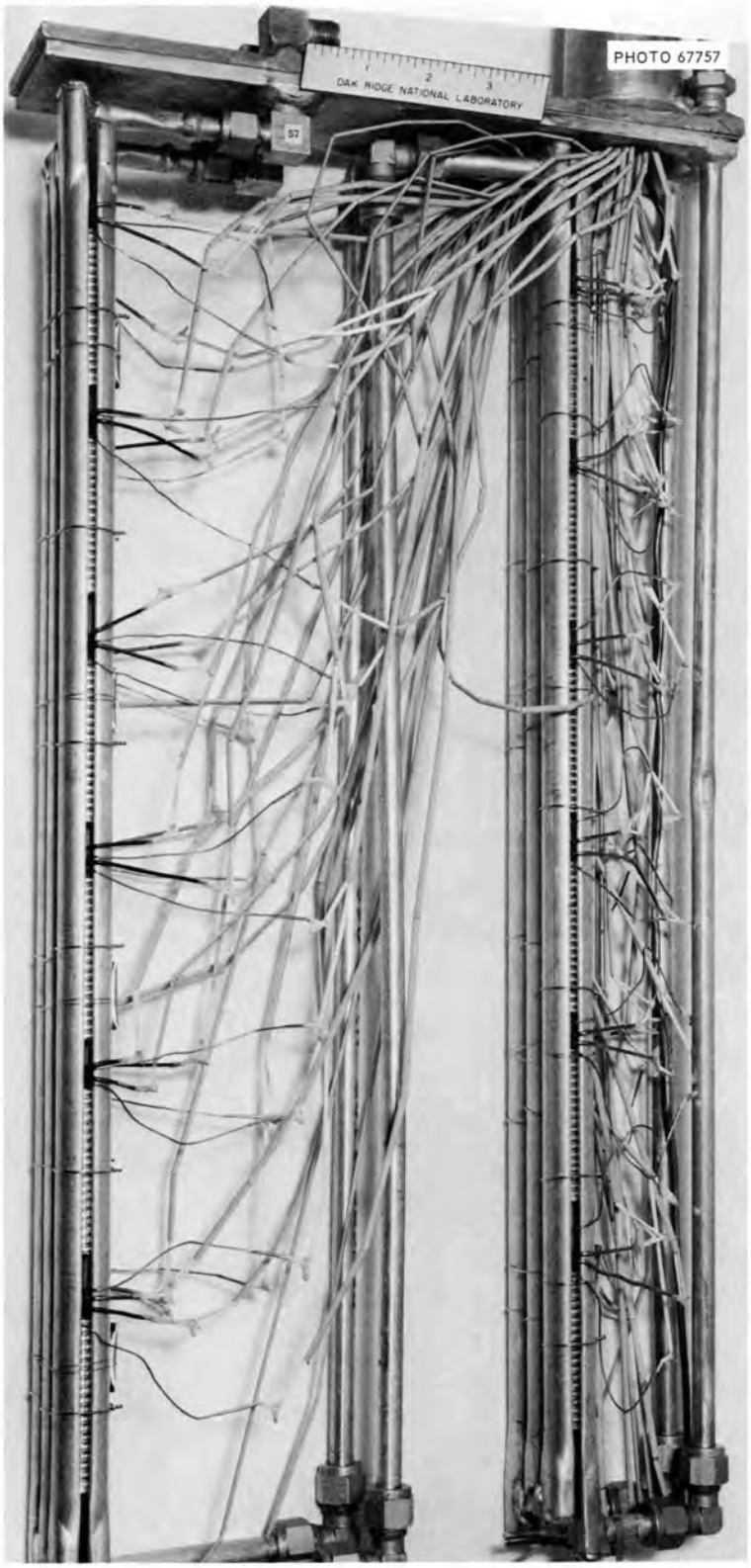

Fig. 5.11. Completed Assembly of ORR Poolside Experiment, ORR-57, Prior to Enclosure.

[redacted]

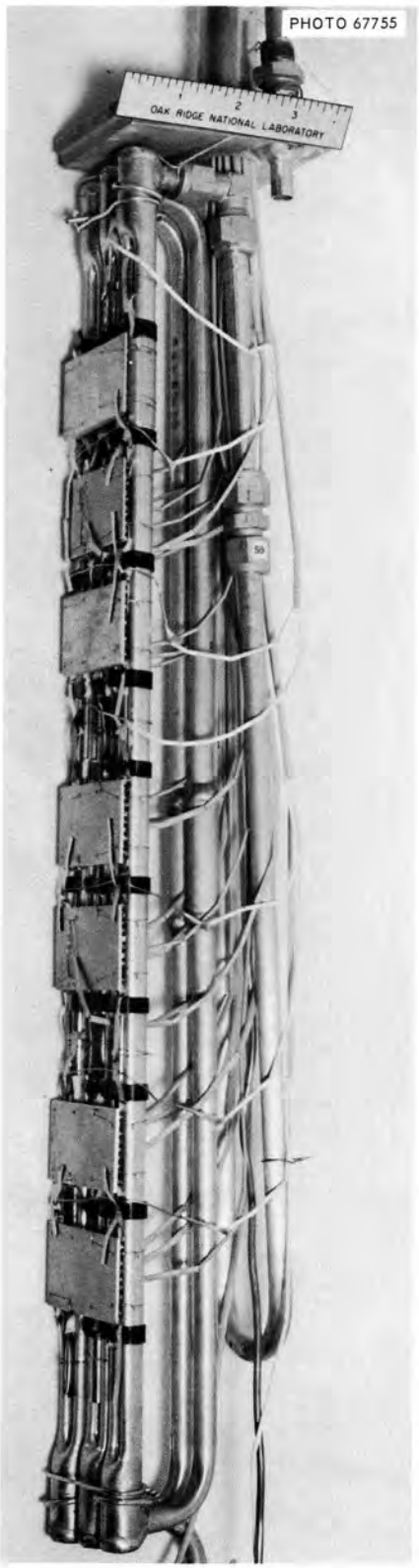

Fig. 5.12. Completed Assembly of ORR Piggyback Experiment, ORR-59, Prior to Enclosure.

[redacted]

yield and flow stresses are intimately associated with the ductile-to-brittle transition observed in these and other body-centered cubic metals, an understanding of the strain-rate sensitivity of yield and flow stresses of irradiated and unirradiated Ferrovac E is applicable to the brittle fracture problem.

Ferrovac E control samples of the two grain sizes mentioned previously have been tested at a series of strain rates between 5×10^{-5} min^{-1} and 2.0 min^{-1}. The true stress—true strain data for the coarse grain material tested at four strain rates are shown in Fig. 5.13.

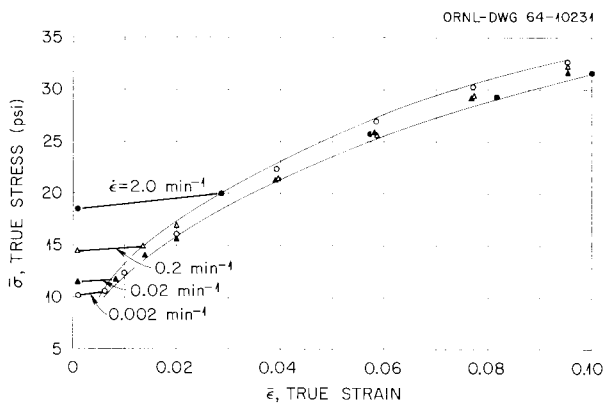

Fig. 5.13. True Stress—True Strain Curves for Ferrovac E at Various Strain Rates. Deformation temperature, 23°C. Grain diameter, 0.18 mm.

The usual increase of lower yield stress and Lüders strain is observed. However, the flow stresses do not increase with increasing strain rate as expected but exhibit a random strain-rate sensitivity. A nearly normal strain-rate sensitivity was observed for the flow stresses of fine grained Ferrovac E.

In Fig. 5.14 the lower yield stress, σ_{LY}, is plotted vs the reciprocal square root of the grain radius, $d^{-1/2}$, for both grain sizes of Ferrovac E at five strain rates. The data indicate that at low strain rates, up to 2×10^{-2} min^{-1}, the friction stress, σ_o, does not change with strain rate while at the higher strain rates, σ_o increases with strain rate. Also, there is a slight indication that the grain size

[redacted]

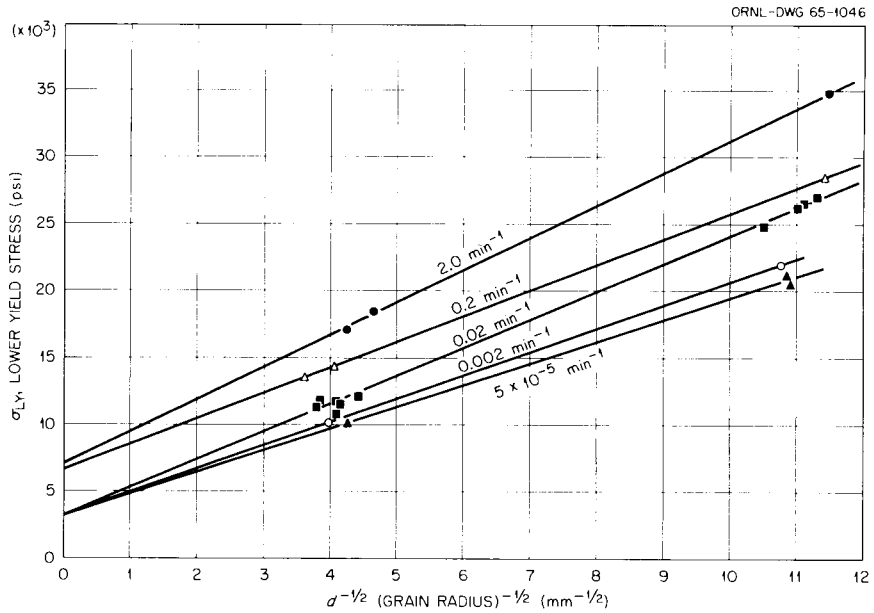

Fig. 5.14. Lower Yield Stress vs (Grain Radius)$^{-1/2}$ for Ferrovac E Vacuum Annealed and Furnace Cooled and Tested at Designated Strain Rates; test temperature, 25°C.

dependence of the lower yield stress decreases at the lower strain rates (i.e., the constant k_y decreases indicating a strain rate sensitivity for this factor).

If an average stress-strain curve was drawn through the homogeneous flow curves of Fig. 5.13, the data could be defined by the generalized work-hardening expression

$$\overline{\sigma} = K\overline{\epsilon}^{n} \quad , \tag{23}$$

where $\overline{\sigma}$ and $\overline{\epsilon}$ are the true stress and true strain, respectively, and K and n, both material constants, are the stress at unit strain and the work-hardening coefficient, respectively. Since the Lüders strains also fall approximately on this average true stress—true strain curve, they also must fit such an expression. Therefore, the log of the lower yield stress, σ_{LY}, is plotted vs the log of the true Lüders strain, $\overline{\epsilon}_L$, in Fig. 5.15 for samples having different grain sizes, different intragranular structure (α and γ heat treatments) and tested at different

[redacted]

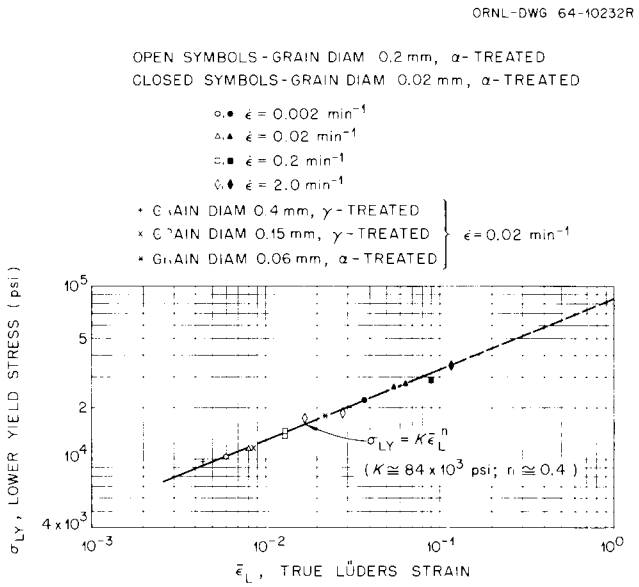

Fig. 5.15. Lower Yield Stress vs True Lüders Strain for Ferrovac E at 23°C for Various Grain Sizes and Strain Rates.

strain rates. The straight line indicates a fit with the expression

$$\sigma_{LY} = K\bar{\epsilon}_L^{\,n} \quad , \tag{24}$$

where K is equal to 84×10^3 psi and n is approximately 0.4.

Data obtained from irradiated samples will be compared with these data on control samples to determine how the strain-rate sensitivity and the Lüders strain characteristics are affected by the radiation damage.

Hydrogen in Steels

R. G. Berggren

Hydrogen is an undesirable constituent in iron and steel since it can lead to embrittlement, loss of strength, cracking, blistering, and decarburization.[33,34] Sources of hydrogen in a nuclear pressure vessel

[33]A. R. Elsea and E. E. Fletcher, Hydrogen-Induced, Delayed, Brittle Failures of High-Strength Steels, DMIC Report 196 (Jan. 20, 1964).

[34]E. E. Fletcher and A. R. Elsea, The Effects of High Pressure, High-Temperature Hydrogen on Steel, DMIC Report 202 (Mar. 26, 1964).

include: hydrogen present in the reactor coolant (usually water), radiolytic decomposition of the coolant (water), corrosion, and nuclear transmutation [(n,p) reactions]. The first three sources have been discussed by Harries and Broomfield.[35] The fourth listed source of hydrogen is discussed in this report. Also included is a description of an experiment designed to test the effect of gamma radiation on hydrogen permeability in steel.

Rate of Hydrogen Production by Transmutation in Pressure-Vessel Steel

Fast neutrons produce hydrogen in many metals by (n,p) reactions with atoms of the metal. The rate of hydrogen production is given by the expression:

$$\frac{dN_i}{dt} = M_i \bar{\sigma}_i \phi \quad , \tag{25}$$

where N_i is the number of atoms of hydrogen arising from reactions with the ith isotope, M_i is the number of atoms of ith isotope, $\bar{\sigma}_i$ is the (n,p) cross section of the ith isotope averaged over the neutron spectrum, and ϕ is the neutron flux. Equation (25) may be written

$$\frac{dN_i}{dt} = A_i N \bar{\sigma}_i \phi \quad , \tag{26}$$

where A_i is the fractional abundance of the ith isotope and N is the total number of atoms.

This expression leads to an overestimate of N_i, since it neglects the burnup of the ith isotope. Thus, it is conservative in that it gives an underestimate of the neutron flux necessary to produce hydrogen attack.

Assuming a fission neutron spectrum and a 1% Mn steel, the rate of production of hydrogen is given in Table 5.1. The contributions of other elements will be insignificant.

---

[35] D. R. Harries and G. H. Broomfield, Hydrogen Embrittlement of Steel Pressure Vessels in Pressurized Water Reactor System, AERE-R 4194, (Sept. 1962).

Table 5.1. Production of Hydrogen in Steel by Transmutation

Element	Isotope	A_i Abundance in Element	$\bar{\sigma}(n,p)^a$ (mb)	$A_i\bar{\sigma}_i = \frac{1}{N\phi}\frac{dN_i}{dt}$ (cm^2)
Iron	54	0.058	66	3.8×10^{-27}
	56	0.917	0.87	0.8×10^{-27}
	57	0.022	7.4	0.16×10^{-27}
	58	0.0033	0.01	3×10^{-32}
Manganese	55	1.000	0.4	4×10^{-30}
			Total	4.76×10^{-27}

[a]J. C. Roy and J. J. Hawton, Table of Estimated Cross Sections for (n,p), (n,α), and (n,2n) Reactions in a Fission Neutron Spectrum, CRC-1003 (Dec. 1960); R. J. Howerton, et al., Thresholds of Neutron Induced Reactions, UCRL-14000 (May 1964), and J. W. Boldeman, "Fission Spectrum Averaged Cross Sections of Threshold Reactions," J. Nucl. Energy 18, 417 (1964).

The Minimum Neutron Flux Necessary to Produce Hydrogen Attack

Permanent embrittlement of steels can be caused by the chemical effects of hydrogen attack and usually occurs in three stages: (1) diffusion of atomic hydrogen into the steel; (2) decarburization by reaction of the hydrogen with iron carbide and forming methane; and (3) intergranular fissuring or blistering of the steel due to the formation of high-pressure methane pockets. The first stage of hydrogen attack is considered to be temporary because ductility can be restored by a relatively low-temperature treatment. Permanent, irreversible embrittlement results when the attack has progressed to the second and third stages.

Based on experience in the chemical industries, Nelson and Effinger[36] and Nelson[37] have defined what were considered the safe operating limits for carbon and various low-alloy steels in hydrogen

[36]G. A. Nelson and R. T. Effinger, "Blistering and Embrittlement of Pressure Vessel Steels by Hydrogen," Welding J. (N. Y) 34, 12s (1955).

[37]G. A. Nelson, "Revisions to Published Chart: Metals for High Pressure Hydrogenation Plants," J. Eng. Ind., Series B, 81, 92 (1959).

service. At atmospheric pressure, decarburization does not occur below 510°C in carbon steel. At higher pressures, hydrogen attack can occur at temperatures as low as 230°C. At 316°C, the minimum pressure for hydrogen attack is 12.6 atm. The solubility of hydrogen in iron and steel[38,39] at this temperature and pressure is 4.3×10^{-2} cm^3 H_2/cm^3 Fe (2.9×10^{-5} atoms H/atom Fe). This value represents the minimum hydrogen solubility for the operating limits defined by Nelson and Effinger.[36,37]

This minimum hydrogen concentration permits the calculation of minimum neutron fluxes required for attack of carbon steel by hydrogen from (n,p) reactions. Other sources of hydrogen will not be considered here. If diffusion is neglected, the values in Table 5.1 and the minimum hydrogen concentration given above for hydrogen attack give a minimum fission neutron dose of 6×10^{21} neutrons/cm^2 required to produce hydrogen attack. However, at temperatures above 230°C where hydrogen attack has been observed, hydrogen diffuses rapidly in steels. For purposes of calculation and illustration, the following assumptions are made:

1. an infinite steel plate of thickness X;
2. hydrogen generated uniformly and at constant rate, R, in the plate by (n,p) reactions;
3. zero partial pressure of hydrogen outside the plate;
4. constant temperature, T;
5. diffusion constant, D, independent of hydrogen concentration, C;
6. hydrogen concentration in the plate surface in equilibrium with gas phase (C = 0 at surface);
7. steady-state conditions.

Fick's second law gives the rate of change of solute concentration at any point in the solvent:

---

[38]A. Sieverts, Z. Physk. Chem. 77, 591 (1911)

[39]R. H. Fowler and C. J. Smithells, Proc. Roy. Soc. (London), Ser. A 160, 37 (1937).

$$\frac{\partial c}{\partial t} = D \frac{\partial^2 c}{\partial x^2} \quad , \tag{27}$$

where c = solute concentration, x = distance from one face of the plate, and D = diffusion coefficient.

Assumption (2) applied to Eq. (27) yields:

$$\frac{\partial c}{\partial t} = D \frac{\partial^2 c}{\partial x^2} + R \quad . \tag{28}$$

The boundary conditions for the above equation are:

a) $\frac{\partial c}{\partial t} = 0$;

b) at $x = \frac{X}{2}$; $\frac{\partial c}{\partial x} = 0$;

c) at $x = 0, X$; $c = 0$.

By boundary condition (a);

$$\frac{\partial^2 c}{\partial x^2} = -\frac{R}{D}$$

Integrating and applying boundary conditions (b) and (c):

$$C_{max} = \frac{RX^2}{8D}; \text{ at center of plate} \quad . \tag{29}$$

From Table 5.1.

$$R = \frac{1}{N}\frac{dNi}{dt} = 4.8 \times 10^{-27}\ \phi\ \text{sec}^{-1}$$

and, as derived above, the critical hydrogen concentration is:

$$C_{max} = 2.9 \times 10^{-5} \quad .$$

Substituting these in Eq. (29) gives the critical fission neutron flux:

$$\phi_c = 4.8 \times 10^{22} \frac{D}{X^2} \quad . \tag{30}$$

Table 5.2 presents representative values of critical fission neutron flux for typical pressure vessel thicknesses and temperatures. These values are based on Eq. (30) and diffusivities, D, of hydrogen

Table 5.2. Typical Critical Fission Neutron Fluxes for Hydrogen Attack in Carbon Steel Pressure Vessels

Temperature (°C)	Diffusivity (cm^2 sec^{-1})	Wall Thickness (cm)	Wall Thickness (in.)	Critical Flux, Φ_c (neutrons cm^{-2} sec^{-1})
250	8.4×10^{-5}	25.4	10	6.2×10^{15}
		12.7	5	2.5×10^{16}
		10.2	4	3.9×10^{16}
275	9.3×10^{-5}	25.4	10	6.9×10^{15}
		12.7	5	2.8×10^{16}
		10.2	4	4.3×10^{16}
300	1.00×10^{-4}	25.4	10	7.3×10^{15}
		12.7	5	2.9×10^{16}
		10.2	4	4.5×10^{16}
400	1.38×10^{-4}	25.4	10	1.0×10^{16}
		12.7	5	4.1×10^{16}
		10.2	4	6.4×10^{16}

in alpha-iron reported by Sykes, Burton, and Gegg.[40] It is seen that hydrogen attack in carbon steel arising from the hydrogen produced in (n,p) reactions would require fluxes above 10^{15} neutrons cm^{-2} sec^{-1}. These levels are higher than those found in the present-day reactors.

Hydrogen Permeability of Steel in a Radiation Environment

Voids containing high-pressure hydrogen may form by several mechanisms. Zapffe and Sims[41,42] proposed that hydrogen embrittlement is the phenomenon of occlusion of molecular hydrogen under high pressure in voids.

[40] C. Sykes, H. Burton, and C. C. Gegg, "Hydrogen in Steel Manufacture," J. Iron and Steel Inst. (London) 156, 155 (1947).

[41] C. A. Zapffe and C. E. Sims, "Defects in Weld Metal and Hydrogen in Steel," Welding J. (N. Y.) 19, 377s (1940).

[42] C. A. Zapffe and C. E. Sims, "Hydrogen Embrittlement, Internal Stress, and Defects in Steel," Trans. AIME 145, 225 (1941).

When the occlusion pressure exceeds the elastic strength of the steel, slip and cleavage planes operate much as during cold deformation. Although there are numerous objections to this "planar pressure" theory, it appears a satisfactory explanation for hydrogen embrittlement phenomena such as hairline cracking.[43] Inglis and Andrews[44] found that when the tensile stress was high and the temperature was just high enough to cause hydrogen attack, fissuring would proceed ahead of decarburization. Holes, fissures, and microcracks may be formed when steels containing hydrogen are cooled through the Ar_1 temperature[43] or rapid temperature fluctuations are experienced.[45] Thus hydrogen attack at temperatures below 250°C may be the result of accumulation of hydrogen gas at inclusions and other defects. Diffusion of hydrogen out of the gas pocket is difficult since the gas must be dissociated from molecular to atomic hydrogen before diffusion can occur. Since nuclear radiation causes dissociation of hydrogen, the hydrogen permeability of metals might be considerably higher in a radiation field than in the absence of radiation. Higher permeabilities would limit pressures in gas pockets to lower values and lessen tendencies to cracking and blistering.

Large increases of hydrogen permeability are probably necessary for marked effects on cracking and blistering of metals due to hydrogen attack. Therefore, a simple series of experiments was conducted to investigate the effects of radiation on hydrogen permeability. The gamma radiation from a ^{60}Co source (gamma-ray energy, 1.25 Mev) should be quite effective in dissociating hydrogen gas. Concurrent ionization effects would also occur. The experimental apparatus consisted of a 12-ft, 10-in.-length of type 304 stainless steel capillary tubing (0.6-mm ID, 0.5-mm wall) wound in a tight coil. The volume of the tube and the pressure transducers was 27 cm^3. The experiment coil was contained in a temperature-controlled resistance heater that would fit

---

[43]M. Szczepanski, p. 174 in The Brittleness of Steel, John Wiley and Sons, Inc., New York, 1963.

[44]N. P. Inglis and W. Andrews, "The Effect on Various Steels of Hydrogen at High Pressures and Temperatures," J. Iron and Steel Inst. (London) 128, 383 (1933).

[45]E. E. Fletcher and A. R. Elsea, The Effects of High Pressure, High-Temperature Hydrogen on Steel, DMIC Report 202 (Mar. 26, 1964).

[redacted]

into the gamma facility. Automatic control and recording of temperature were utilized. The apparatus was flushed and filled with hydrogen gas at about 20 atm abs pressure and sealed off. Leak rates at room temperature were determined for periods from 2 to 72 hr and were less than 0.25 cm^3/hr in all runs. The test section was then brought to test temperature and leak rates were determined. The test section was then lowered into the gamma field of 3.2×10^6 r/hr, and leak rates determined at the same temperature. The apparatus remained sealed throughout the three steps of the test. The apparatus was then repressurized, and the identical procedure was followed for the next test temperature.

The quantity of hydrogen per unit time, J, passing through a column of unit cross sectional area and unit thickness is given by Fick's first law:

$$J = -D \frac{\partial c}{\partial x} \quad , \tag{31}$$

where D is the diffusion coefficient, assumed independent of c; c is the solute concentration, and x is the distance along the diffusion path.

For diffusion of hydrogen from the interior to the exterior of a thick-walled tube of length, ℓ, Eq. (31) may be written:

$$\frac{Q}{A} = -D \frac{\partial c}{\partial x} \quad , \tag{32}$$

where Q is the hydrogen leaking through the tube wall per unit time.

$A = 2\pi x \ell$, the area at radius x.

Substituting and integrating:

$$\frac{Q}{2\pi \ell} \ln \left(\frac{r_2}{r_1}\right) = -D(c_2 - d_1) \quad , \tag{33}$$

where $r_1 = 0.3$ mm, $r_2 = 0.8$ mm, c_1, c_2 are hydrogen concentrations at the corresponding radii.

Assume: $c_2 = 0$ at the outer wall of tube, $c_1 = S$, solubility of hydrogen in austenitic stainless steel at test temperature and pressure. Then, for the geometry of this experiment:

[redacted]

[redacted]

$$D = 4 \times 10^{-4} \frac{Q}{S} \quad (cm^2/sec) \quad , \tag{34}$$

where D is the apparent diffusion coefficient. This apparent diffusion coefficient will include surface effects.

The experimentally determined diffusivities are presented in Table 5.3. The results are presented in historical sequence. Several leak rates were determined at room temperature prior to the experimental runs presented in the table and were essentially zero both in and out of the gamma field. The scatter of the results was greater than the average change in apparent diffusion coefficient. The last column in Table 5.3 lists estimated accuracies based on maximum room temperature leak rates and sensitivity of the pressure measuring system.

The apparent diffusion coefficients in the absence of a radiation field are in good agreement (less than ±50%) with an extrapolation (Fig. 5.16) of values published by Geller and Sun.[46]

The relatively small observed changes in D may be due to a high recombination rate forming molecular from atomic hydrogen. The change in partial pressure of atomic hydrogen (H_1) in molecular hydrogen (H_2) may be measured by placing a sealed capsule in the gamma field. A thick wall capsule (volume = 25 cm^3) was pressurized, sealed, and placed in the gamma field. No observable pressure rise was recorded. The sensitivity of the apparatus was such that 7% H_1 in H_2 could have been recorded. Thus the partial pressure of H_1 in the test series was less than 1.4 atm.

---

[46]W. Geller and T. H. Sun, "Effect of Alloying Additions on the Diffusion of Hydrogen in Iron and Contribution to the Iron-Hydrogen System," Arch. Eisenhuettenw. 21, 423 (1950).

[redacted]

Table 5.3. Effect of Gamma Radiation on Hydrogen Permeability of Type 304 Stainless Steel

Test Number[a]	Temperature (°K)	Average Pressure (atm abs)	Leak Rate (cm^3/hr)	Hydrogen[b,c] Solubility $S(cm^3/cm^3)$	Apparent D (cm^2/sec)	Delta D (%)	Estimated Accuracy (%)
1A	700	18.0	12.0	1.29	1.03×10^{-6}		+12, −14
2A	755	16.6	27.6	1.84	1.67×10^{-6}		+20, −21
3A	589	19.1	1.6	0.50	3.6×10^{-7}		+10, −26
3B	589	20.8	2.64	0.51	5.7×10^{-7}	+58	+20, −29
4A	644	20.0	4.50	0.88	5.7×10^{-7}		+12, −18
4B	644	18.3	5.22	0.87	6.7×10^{-7}	+17	+11, −16
5A	589	21.2	0.75	0.525	1.58×10^{-7}		+140, −173
5B	589	20.3	1.79	0.515	3.9×10^{-7}	+148	+30, −44
6A	589	20.4	1.42	0.515	3.1×10^{-7}		+25, −43
6B	589	18.2	1.25	0.496	2.8×10^{-7}	−10	+18, −38
7A	644	19.7	4.90	0.88	6.2×10^{-7}		+40, −45
7B	644	18.4	4.69	0.83	6.3×10^{-7}	+2	+13, −18
8A	689	20.7	6.42	1.29	5.5×10^{-7}		+70, −74
8B	689	19.2	8.40	1.24	7.5×10^{-7}	+36	+3, −6
					Average	+42	

[a]A tests were in absence of radiation field and B tests were in gamma radiation field.

[b]A. Sieverts, Z. Physk. Chem. 77, 591 (1911).

[c]M. H. Armbruster, "Hydrogen in Fe, Ni, and Certain Steels, Solubilities at Low Pressures from 400°C to 600°C," J. Amer. Chem. Soc. 65, 1043 (1943).

[redacted]

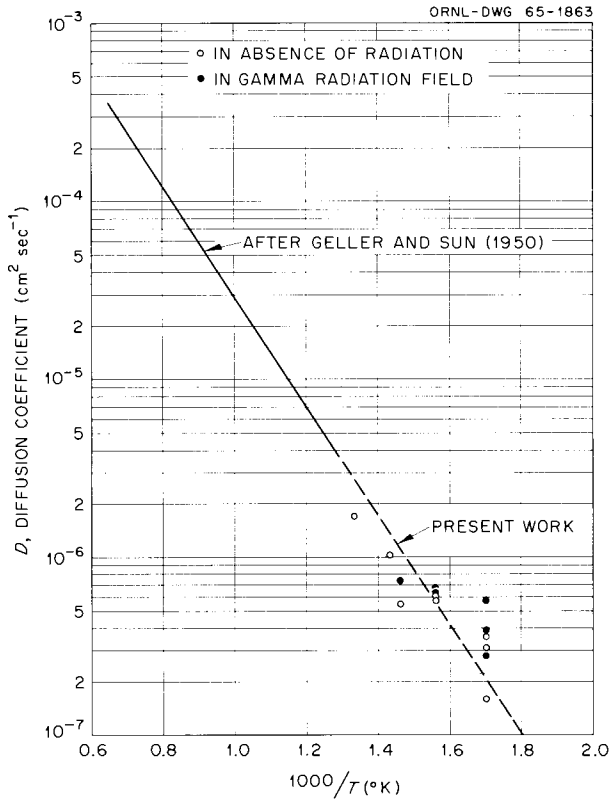

Fig. 5.16. Diffusion Coefficient for Hydrogen in 18-8 Stainless Steel.

SM-1 Pressure Vessel Surveillance Program

R. G. Berggren

The third surveillance capsule, containing subsize Izod impact samples has been removed from the SM-1 Reactor at Fort Belvoir, Virginia, after 25.6 Mwyr of reactor operation. Prior surveillance tests were conducted after 16.4 and 20.8 Mwyr of reactor operation.[47] The subsize Izod impact tester required overhaul after several years of storage but is now ready for the test series.

---

[47]R. G. Berggren and L. D. Schaffer, "SM-1 Pressure Vessel Surveillance Program," Quarterly Progress Report: Irradiation Effects on Reactor Structural Materials, HW-83398, p. 10.23 (Aug. 15, 1964).

[redacted]

Impact Tests on Irradiated Pressure Vessel Steels

R. G. Berggren W. J. Stelzman T. N. Jones

A series of accelerated irradiations have been carried out in the poolside facility of the ORR on Charpy V-notch impact samples of ASTM A-212, grade B, steel. These experiments are intended primarily to determine the radiation embrittlement in synthetic heat-affected-zone material simulating the heat-affected zones near welds in actual reactor pressure vessels. In addition to the synthetic heat-affected-zone samples, notch impact and tensile samples of baseplate material are being included in these experiments. The design of elevated temperature capsules is also being investigated.

Experiment ORR-10 contained 10 heat-affected-zone and 40 baseplate impact specimens. Temperature distribution in this experiment was non-uniform and was higher (345 to 400°C) than desired. Experiment ORR-58 contained 50 Charpy V-notch impact specimens of synthetic heat-affected-zone material (20 specimens) and baseplate material (30 specimens). Guard heaters were incorporated to reduce temperature gradients at the ends of the capsule. Exposure temperatures of 455 to 510°C in this experiment were also higher than desired. Failure of one guard heater at startup and one main heater one week later made temperature control difficult. Improvements in the heaters were incorporated in experiment ORR-61 and exposure temperatures of (230 ± 15)°C were obtained. This experiment contained 14 tensile specimens and 34 Charpy V-notch impact specimens of baseplate material. Experiment ORR-62 contained 21 tensile specimens and 27 Charpy V-notch impact specimens of baseplate material and operated at (280 ± 10)°C. Experiment ORR-63 contained 48 Charpy V-notch impact specimens of baseplate material for recovery studies. A temperature excursion to greater than 540°C at reactor startup was found by later hot-cell examination to have damaged the Inconel-X leaf springs.

After the initial temperature excursion, exposure temperatures were controlled at (360 ± 45)°C. Experiment ORR-69 contained 48 tensile test specimens for recovery studies. Exposure temperatures were (295 ± 10)°C. Further irradiations of synthetic heat-affected-zone specimens of pressure vessel steels are planned.

As is described immediately below, the impact machine has now been calibrated in accordance with the specifications of several agencies. The irradiated samples will be tested as soon as the machine is installed in the hot cells.

Hot-Cell Equipment

R. G. Berggren W. J. Stelzman T. N. Jones

The errors encountered in calibration of the Charpy V-notch impact test machine[48] have been corrected and the machine now meets ASTM standards and Army Materials Research Agency (AMRA) requirements. Table 5.4 compares the ORNL calibration results with standard calibration values supplied by AMRA. Modification of the machine for remote specimen handling and test temperature control is almost completed and will not affect the machine calibration. The testing machine vendor is presently modifying the pendulum of the second machine.

[48]R. G. Berggren, W. J. Stelzman, and T. N. Jones, "Charpy Impact Machine Calibration," Quarterly Progress Report: Irradiation Effects on Reactor Structural Materials, HW-83398, p. 10.29 (Aug. 15, 1964).

Table 5.4. Calibration Tests on ORNL Charpy V-Notch Impact Machine

Type of Sample	Impact Energy		Variations	
	AMRA Standard Average Value (ft-lb)	ORNL Measured Average Value (ft-lb)	Allowed by AMRA	ORNL Observed
High energy	84.4	84.5	±5.0%	+0.2%
Medium energy	47.5	49.4	±5.0%	+4.0%
Low energy	12.7	13.2	±1.0 ft-lb	+0.5 ft-lb

The remotely operated Instron tensile test machine has been equipped with an improved extensometer calibrator (Fig. 5.17). Modifications to the extensometer include a remotely operated elevator to position the extensometer on the test sample, removable zero stops, an improved transducer and mounting, and zero suppression and span circuitry. The remotely operated extensometer calibrator permits calibration settings to within 20 μ in. with a screw accuracy of 10 μ in. Overall accuracy of the extensometer system meets ASTM Class B-1 up to an extension of 0.028 in., Class B-2 up to an extension of 0.100 in., and Class C up to an extension of 0.150 in.

An inert atmosphere recovery furnace for temperatures to 540°C has been calibrated and installed in the hot cells.

A Converter Facility for Providing Fission-Spectrum Neutrons in the Bulk Shielding Reactor

W. E. Brundage

Studies of the effect of neutron irradiation on metals and alloys generally require that the neutron spectrum be known. Measurements of the spectrum are difficult to make and, in the usual reactor experimental facility, the spectrum is subject to changes caused by variations in fuel and experiment loading of the reactor. One method of overcoming this difficulty is to irradiate specimens in a flux of pure fission energy neutrons since this spectrum is well known.[49] A fission spectrum facility is being designed for the Bulk Shielding Reactor.

[49] J. A. Grundl, Study of Fission Spectra with High-Energy Activation Detectors, LAMS-2883 (May 20, 1963).

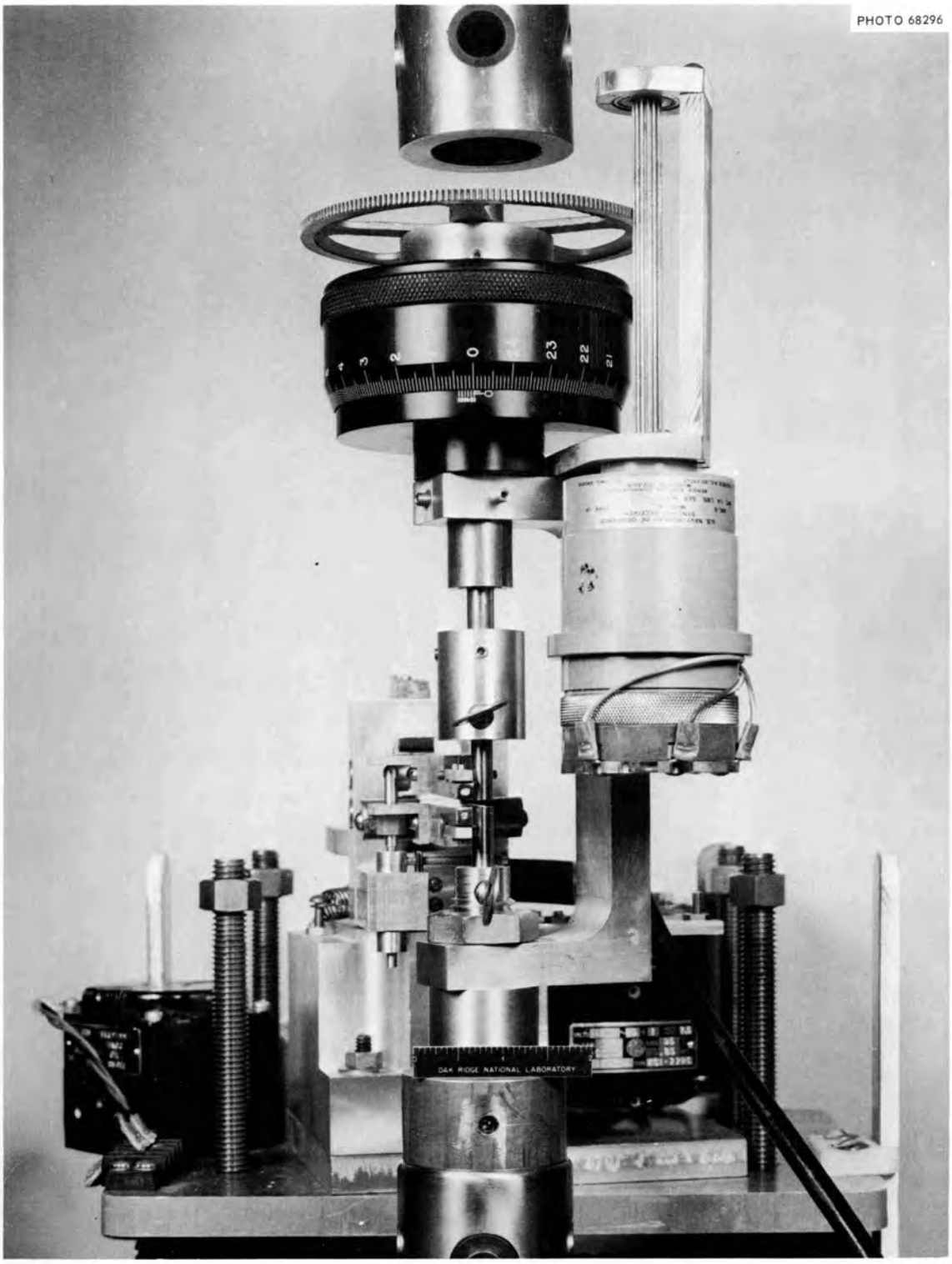

Fig. 5.17. Remotely Controlled Extensometer and Extensometer Calibrator in Calibration Position.

[redacted]

The facility as presently conceived is schematically illustrated in Fig. 5.18. Figure 5.19 is a section through the sample chamber and converter tube. The space available, inside the tube, for experiments will have a diameter of 3 in. and a length of 12 in.

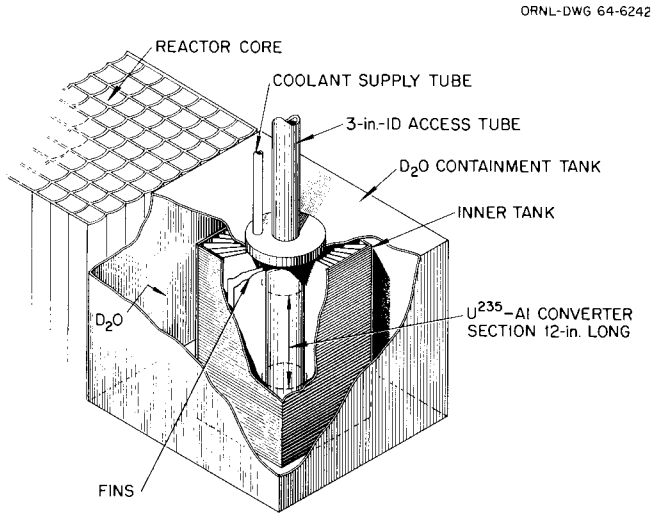

Fig. 5.18. Section of Fission-Spectrum Facility.

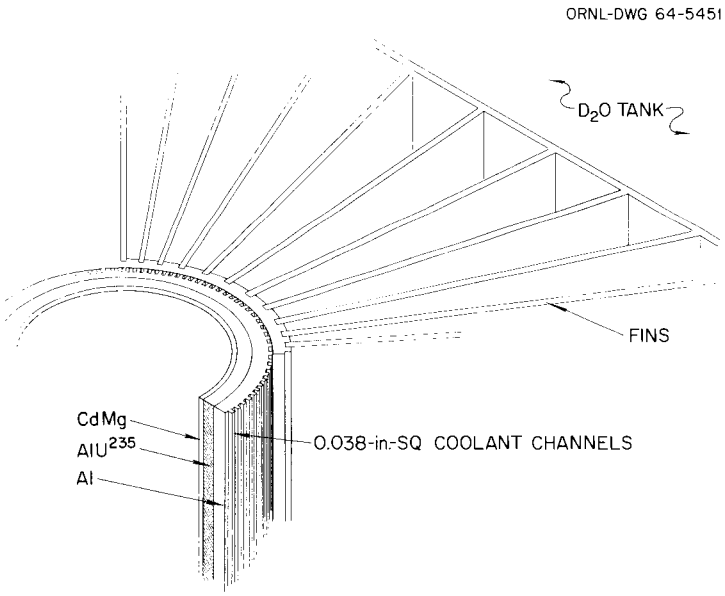

Fig. 5.19. Section Through Sample Chamber and Converter Tube.

[redacted]

The facility will be permanently located in the BSR pool in such a manner that the movable reactor can be brought up to the facility for operation. The leakage flux from one face of the reactor is well thermalized by passing through a 24-in.-thick tank of D_2O. The thermal neutrons are captured in a cylindrical converter tube containing ^{235}U, producing fission neutrons that irradiate specimens placed inside the cylinder.

Some of the neutrons generated in the converter tube are reflected back through the sample by the surrounding moderator. Since these have energies below the original emission energy, the spectrum is altered by this feedback. To control this feedback, a nonmoderating region surrounds the tube.[49,50] This has the effect of reducing the probability of the fission neutrons returning to the converter tube and the sample chamber before it has traversed a sufficient length of moderator to be thermalized. Also, the sample will be shielded from the thermal neutrons by the ^{235}U in the converter tube and an inner cylinder of cadmium.

The experiments intended for the facility require that a fission flux of at least 10^{12} neutrons cm^{-2} sec^{-1} be attained. This intensity, coupled with the physical size of the facility establishes a minimum heat generation level in the converter tube of around 30 kw. The utility and safety of the facility is based on the efficient removal of the heat to provide a reasonable ambient temperature for experimental use and to prevent any possibility of a hazard due to melting of the converter tube or its cladding and the resulting release of fission products.

Evaluation of the system revealed that the heat could best be dissipated by using water as a coolant. The minimum volume of water capable of removing the heat was determined, and computer calculations were performed[51] to determine the effect of this volume of moderator at

---

[50]R. R. Coltman, C. E. Klabunde, D. L. McDonald, J. K. Redman, and G. F. Fielder, "Low-Temperature Irradiation Studies," Solid State Div. Ann. Progr. Rept. May 31, 1963, ORNL-3480, p. 57.

[51]The calculations were carried out by J. R. Knight, Oak Ridge Central Data Processing Division.

various points within the void. It was determined that the small volume of water placed close to the converter element would not appreciably alter the neutron spectrum.

If failure of the forced coolant flow occurred during operation, an excessive temperature would be reached in a very short time. To alleviate this condition, a series of radial fins extending across the void were added to provide a thermal path to the surrounding D_2O and water (Fig. 5.18). These fins will protect the converter tube from approaching meltdown temperature but will not provide sufficient cooling for normal experimental requirements.

The preliminary design parameters were used to determine the heat-transfer characteristics of the system. The results of this analysis[52] show that the system is inherently safe and that the wall temperature of the facility could be maintained at 31°C by prechilling the coolant with a 10-ton refrigeration system. Figure 5.20 shows the coolant flow system as presently conceived.

The results of thermal analyses are shown in Table 5.5 for several conditions. The 30-kw design level will represent very conservative operation of the facility.

It will be necessary to consider the nuclear safety characteristics of the system. In order to obtain the desired flux level, an estimated loading of 1.5 kg of ^{235}U will be required, and the system must not be capable of becoming critical under any conceivable condition. On the other hand, the leakage flux from the reactor under equivalent conditions has been measured and is not sufficient to generate the required fission flux. The solution to this problem lies in the moderation and feedback of the fission neutrons to the converter tube. The system is a subcritical assembly and acts as a neutron flux amplifier. The k, or reproduction factor, of the assembly controls the amplification which is $\frac{1}{1-k}$ (ref. 53). For this system an amplification of 4 would be more than sufficient, requiring k = 0.75.

---

[52]G. H. Llewellyn, Design Analysis of a Pure Fission Spectrum Facility for the BSR, ORNL-TM-987 (Jan. 1965).

[53]D. J. Hughes, p. 50 in Pile Neutron Research, Addison-Wesley, 1953.

[redacted]

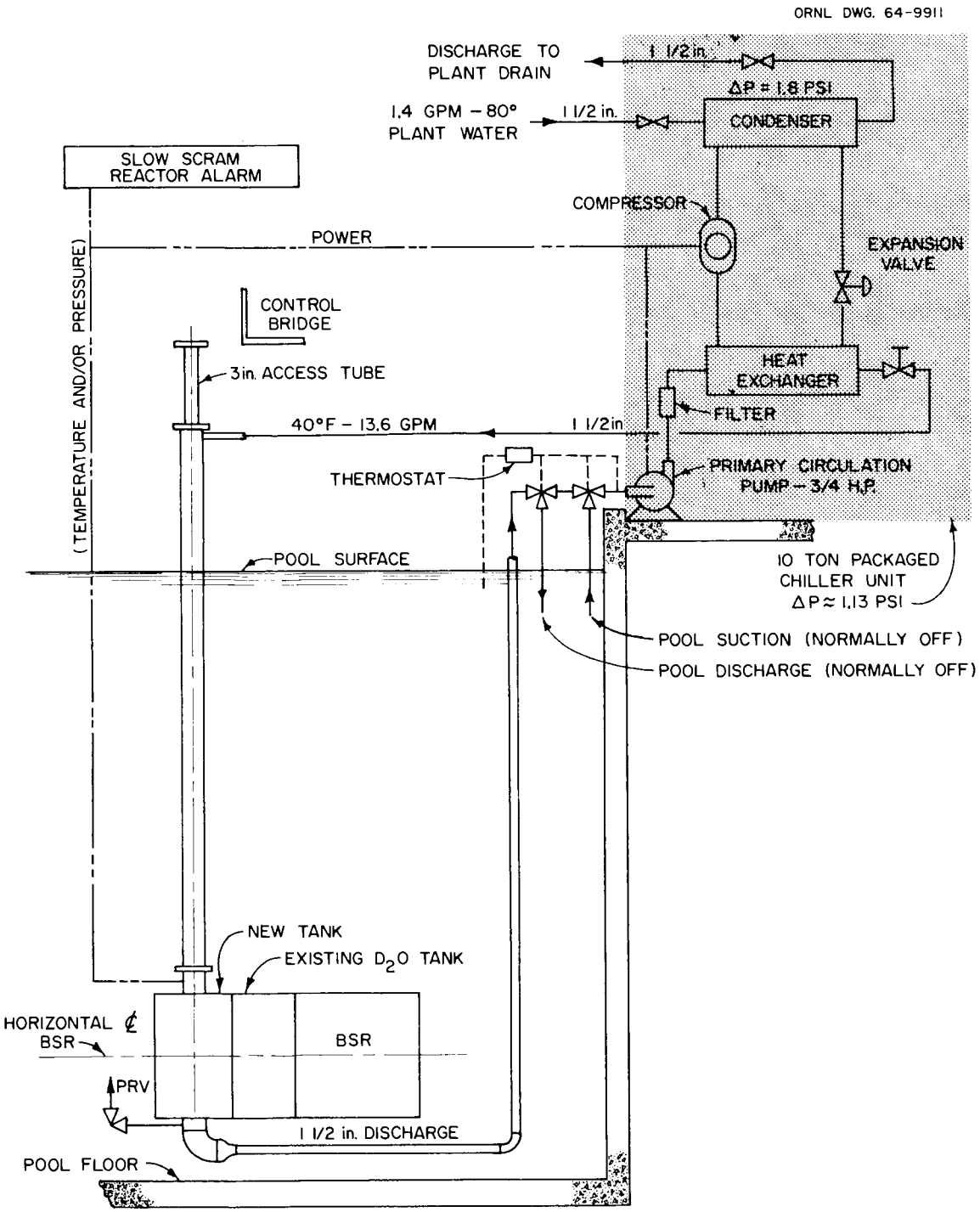

Fig. 5.20. Facility Coolant Flow Diagram.

[redacted]

Table 5.5. Analyses of Heat-Transfer Characterictics

Condition	Power (kw)	Maximum Coolant Channel Wall Temperature (°C)	Maximum Internal Wall Temperature (°C)	Safety Factor
Normal	30.0	17	31	
No coolant flow	77.6	493	530	2.59
Full coolant flow with chiller operating	205.5	127[a]	226	6.84
Full coolant flow without chiller	189.0	127[a]	218	6.30

[a]Limiting temperature.

If the ^{235}U loading of the converter tube can be made this high and still have it safe from accidental criticality from other factors, the system will generate power in proportion to the power level of the BSR. A method of regulating the power generation of the system when the reactor is at steady full power operation is to introduce a layer of light water between the reactor face and the converter. This can be done simply by separating the D_2O tank and reactor from the tank containing the converter (not shown in schematic drawing of Fig. 5.18).

Samples exposed in the facility will be subjected to a flux of 10^{12} fission neutrons and about 2×10^{11} neutrons of intermediate energies. The intermediate energy neutrons contribute only a small portion of the radiation damage since the damage effectiveness of the flux is roughly proportional to the energy. It is estimated that the feedback flux will contribute only 6% of the total damage.

Design work will be continued on the facility with particular attention focused on the nuclear parameters before the detailed design is performed.

BSR Liquid-Nitrogen-Cooled Cryostat

J. T. Howe W. E. Brundage

Several experiments planned for the Bulk Shielding Reactor will require that the specimen be maintained below room temperature. A cryostat is being designed and constructed for these experiments.

The cryostat will be mounted so that it may be moved to various positions within the BSR pool. This will permit the same cryostat to be used for experiments amenable to reactor spectrum neutrons, thermal neutrons, or fission neutrons by positioning the sample chamber against the reactor face, in a thermal column, formed by positioning a tank of D_2O between the cryostat and the reactor, or within the Fission Spectrum Irradiation Facility, respectively. The positioning feature is to be obtained by mounting the cryostat housing and the associated equipment on an existing movable bridge over the BSR pool.

The cryostat, illustrated in Fig. 5.21, will have a space 1 7/8-in. ID and 24 in. long into which experiments or samples may be placed. The temperature of this region can be maintained at any point from room temperature to liquid nitrogen temperature by circulating cooled helium gas through the experimental space. If it is necessary to isolate the experiment from the helium (approx 60 psig), an inner tube will be used to enclose the specimen, reducing the usable volume. Provision will also be made for removing samples under liquid nitrogen.

The flow diagram for the cryostat system is shown in Fig. 5.22. The compressors operate at room temperature, and the cooling is provided by liquid nitrogen through the use of a 20-ft section of a heat-exchanger tube having three coaxial passages. The center and inner annulus form a counter-flow heat economizer for the helium flow and the outer annulus is used for the liquid nitrogen coolant.

The presence of oil vapor introduced into the helium stream by the usual compressor is detrimental to the cryostat since it condenses out in the cold end, blocking the flow passages and when subject to reactor irradiation forms a carbon deposit that cannot be removed. Oil separators are not efficient enough to prevent this, only to slow its progress.

[redacted]

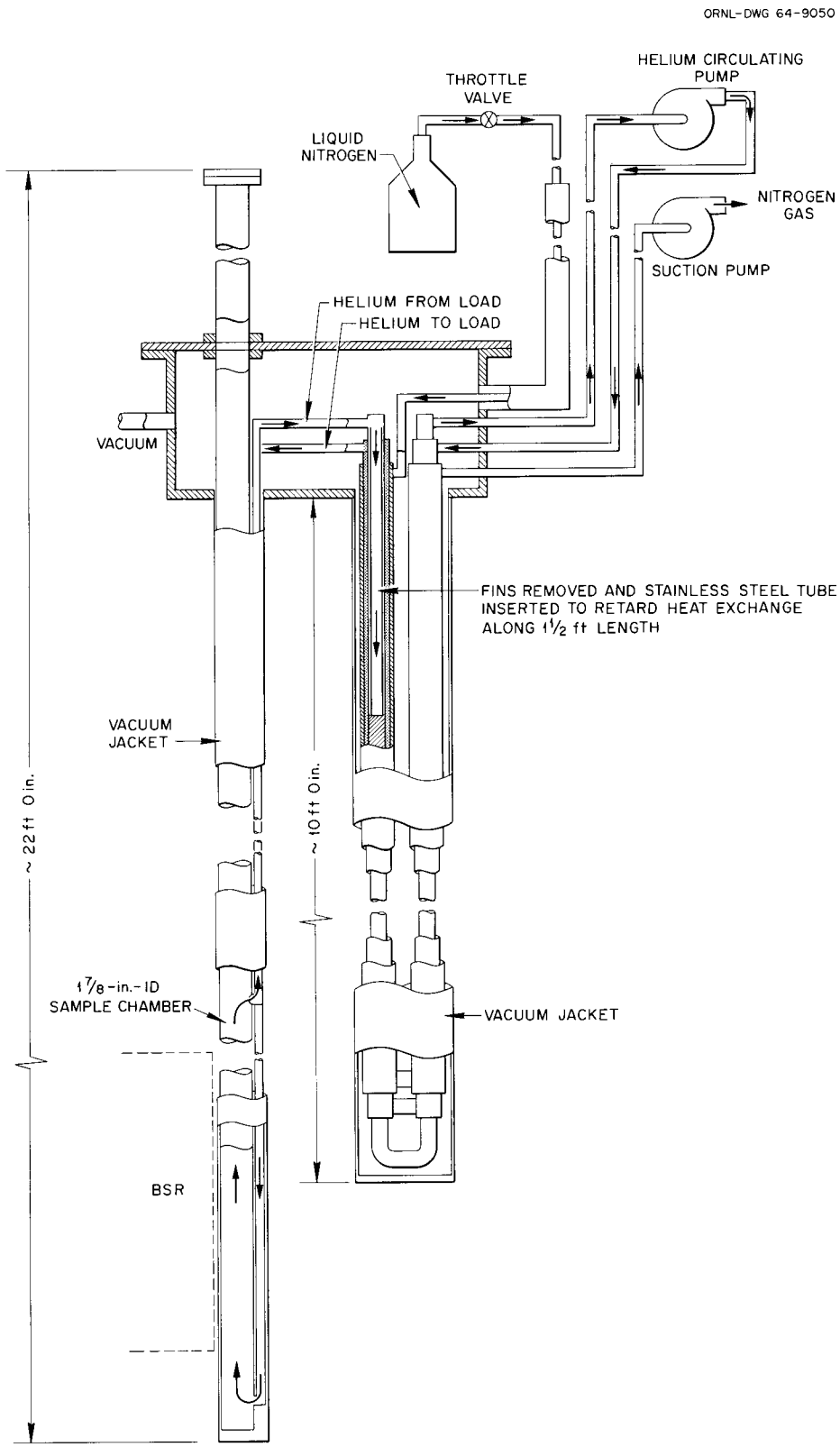

Fig. 5.21. Bulk Shielding Reactor Liquid-Nitrogen-Cooled Cryostat.

[redacted]

[redacted]

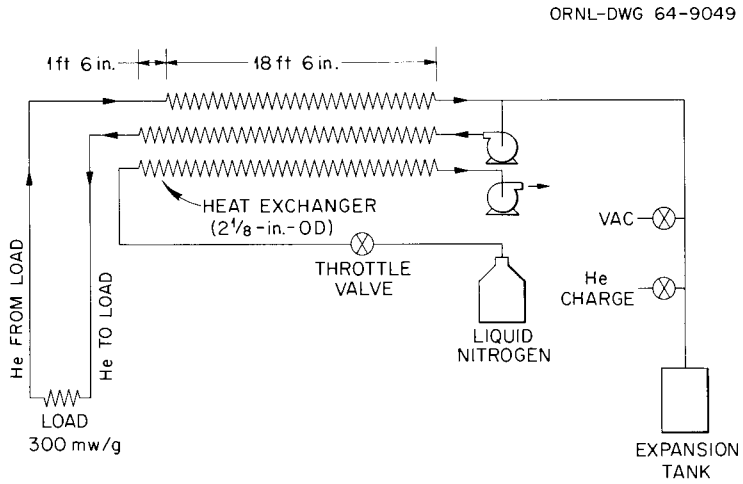

Fig. 5.22. Liquid-Nitrogen-Cooled BSR Cryostat Line Diagram.

Attention is being given to obtaining or developing a suitable sealed, oilless compressor. A sliding graphite-vane sealed blower of appropriate capacity has been obtained for this application.

The graphite vanes will not be suitable since water vapor will also be condensed out of the helium and graphite loses its lubricating properties in the absence of water vapor. It is hoped that a substitute material can be found for the vanes so that the oil problem can be eliminated.

At the present time, the blower is being fitted out for testing alternate vane materials. Three materials are now planned for testing: (1) laminated bakelite, (2) DU Bearing Material,[54] and (3) a bronze impregnated TFE fluorocarbon.

If no satisfactory vane material is found, the circulation will be done with standard refrigeration type compressors used with an oil separating system. This would make the system more bulky, less efficient and, as previously noted, subject to a gradual deterioration of the flow due to blockage of the passages.

---

[54]A proprietary material by Garlock, Inc., New Jersey.

[redacted]

The fabrication of the heat exchanger and cryostat tube assembly is now in progress and should be completed by April 1965. The design of the external portion of the system and the assembly should be completed in time to permit operation of the system by June 1965.

[redacted]

Previous reports in this series are:

ORNL-TM-920	Period Ending June 30, 1964
ORNL-TM-960	Period Ending September 30, 1964
ORNL-TM-1000	Period Ending December 31, 1964

[redacted]

[redacted]

Internal Distribution

1–3. Central Research Library
4–5. ORNL – Y-12 Technical Library
Document Reference Section
6–15. Laboratory Records
16. Laboratory Records, RC
17. ORNL Patent Office
18. G. M. Adamson, Jr.
19. J. C. Banter
20. J. H. Barrett
21. S. E. Beall
22. M. Bender
23. R. G. Berggren
24. J. O. Betterton, Jr.
25. D. S. Billington
26. A. L. Boch
27. B. S. Borie
28. G. E. Boyd
29. W. H. Bridges
30. R. B. Briggs
31. W. E. Brundage
32. J. V. Cathcart
33. G. W. Clark
34. K. V. Cook
35. J. H. Crawford
36. J. E. Cunningham
37. J. H. DeVan
38. C. V. Dodd
39. D. A. Douglas, Jr.
40. J. I. Federer
41. B. E. Foster
42. A. P. Fraas
43. J. H Frye, Jr.
44. R. J. Gray
45. W. R. Grimes
46. J. P. Hammond
47. W. O. Harms
48. R. L. Heestand
49. M. R. Hill
50. N. E. Hinkle
51. H. W. Hoffman
52. H. Inouye
53. T. N. Jones
54. G. W. Keilholtz
55. B. C. Kelley
56. J. A. Lane
57. C. F. Leitten, Jr.
58. A. L. Lotts
59. T. S. Lundy
60. R. N. Lyon
61. H. G. MacPherson
62. R. E. MacPherson
63. M. M. Martin
64. W. R. Martin
65. R. W. McClung
66. H. E. McCoy, Jr.
67. H. C. McCurdy
68. R. E. McDonald
69. D. L. McElroy
70. C. J. McHargue
71. M. C. McIlwain
72. F. R. McQuilkin
73. A. J. Miller
74. E. C. Miller
75. F. H. Neill
76. S. M. Ohr
77. P. Patriarca
78. A. M. Perry
79. S. Peterson
80. M. L. Picklesimer
81. P. L. Rittenhouse
82. M. W. Rosenthal
83. G. Samuels
84. H. W. Savage
85. W. Schüle
86. J. L. Scott
87. O. Sisman
88. G. M. Slaughter
89. G. P. Smith, Jr.
90. S. D. Snyder
91. I. Spiewak
92. J. T. Stanley
93. W. J. Stelzman
94. J. O. Stiegler
95. A. Taboada
96. D. B. Trauger
97. G. M. Watson
98. M. S. Wechsler
99. A. M. Weinberg
100. J. R. Weir
101. W. J. Werner
102. G. D. Whitman
103. J. M. Williams
104. R. O. Williams
105. J. C. Wilson

[redacted]

[redacted]

106. F. R. Winslow
107. H. L. Yakel, Jr.
108. F. W. Young, Jr.
109. C. S. Yust

External Distribution

110–112. F. W. Albaugh, GE, Hanford
113. A. J. Alexander, AEC, CANEL
114. R. J. Allio, Westinghouse Atomic Power Division
115. R. D. Baker, Los Alamos Scientific Laboratory
116. L. Brewer, University of California, Berkeley
117. V. P. Calkins, GE, NMPO
118. W. Cashin, Knolls Atomic Power Laboratory
119. S. Christopher, Combustion Engineering, Inc.
120. R. M. Cilimberg, Division of Reactor Development, AEC Washington
121–122. D. F. Cope, AEC, ORO
123. G. K. Dicker, Division of Reactor Development, AEC, Washington
124. E. A. Evans, GE, Vallecitos
125. W. C. Francis, Phillips Petroleum Company
126. R. G. Grove, Mound Laboratory
127. D. H. Gurinsky, BNL
128. S. Hasko, NBS
129. A. N. Holden, GE, APED
130. J. S. Kane, University of California, Livermore
131. J. H. Kittel, ANL
132. E. J. Kreih, Westinghouse, Bettis Atomic Power Laboratory
133. W. L. Larsen, Iowa State University, Ames Laboratory
134. J. H. MacMillan, Babcock and Wilcox Company
135. R. E. Pahler, Division of Reactor Development, AEC, Washington
136. S. Paprocki, BMI
137. D. Ragone, GA
138. L. M. Raring, Pratt & Whitney, CANEL
139. Division of Research and Development, AEC, ORO
140. A. H. Roberson, U. S. Department of the Interior, Bureau of Mines
141. W. Rostokev, Illinois Institute of Technology Research Institute
142. F. C. Schwenk, Division of Reactor Development, AEC, Washington
143–144. J. M. Simmons, Division of Reactor Development, AEC, Washington
145. L. E. Steele, Naval Research Laboratory
146. R. H. Steele, Division of Reactor Development, AEC, Washington
147. W. F. Sheely, Division of Research, AEC, Washington
148. A. Strasser, United Nuclear Corporation
149. W. R. Voigt, Division of Reactor Development, AEC, Washington

[redacted]

150. C. E. Weber, Atomics International
151. G. W. Wensch, Division of Reactor Development, AEC, Washington
152. M. J. Whitman, Division of Reactor Development, AEC, Washington
153–167. Division of Technical Information Extension